Ion-channel function and cross-species determinants in viral assembly of nonprimate hepacivirus p7

Stephanie Walter[1], Alexander Bollenbach[1], Juliane Doerrbecker[1], Stephanie Pfaender[1], Richard J. P. Brown[1], Gabrielle Vieyres[1], Claire Scott[2], Richard Foster[2], Abhinav Kumar[3], Nicole Zitzmann[3], Stephen Griffin[2], François Penin[4], Thomas Pietschmann[1] and Eike Steinmann[1*]

[1]Institute for Experimental Virology, TWINCORE Centre for Experimental and Clinical Infection Research; a joint venture between the Medical School Hannover (MHH) and the Helmholtz Centre for Infection Research (HZI), Feodor-Lynen-Str. 7, 30625 Hannover, Germany.

[2]Leeds Institute of Cancer & Pathology, University of Leeds, Wellcome Trust Brenner Building, St James' University Hospital, Leeds, Great Britain.

[3]Oxford Glycobiology Institute, Department of Biochemistry, University of Oxford, Oxford, Great Britain.

[4]Insitut de Biologie et Chimie des Protéines, CNRS, UMR 5086, Laboratoire International Associé CNRS-UIUC, Labex Ecofect, University of Lyon, Lyon, France.

Running title: Determinants of nonprimate hepacivirus p7 for ion-channel activity and virus assembly

Keywords: hepatitis C virus, p7, nonprimate hepacivirus, equine hepacivirus, ion-channel

Word count, abstract: 250

Word count, text: 6376

***Contact Information**

PD Dr. Eike Steinmann

Institute for Experimental Virology

TWINCORE, Centre for Experimental and Clinical Infection Research; a joint venture between the Medical School Hannover (MHH) and the Helmholtz Centre for Infection Research (HZI)

Feodor-Lynen-Str. 7, 30625 Hannover, Germany

Phone: +49 511 2200 27134 Fax: +49 511 2200 27139

E-mail: Eike.Steinmann@twincore.de

Abbreviations

CF: carboxyfluorescein

DAA: direct acting antiviral

EI-IRES: encephalomyocarditis virus internal ribosomal entry site

ER: endoplasmic reticulum

FU: fluorescent units

G-Luc: *Gaussia*-Luciferase

GBV-B: GB virus B

GT: genotype

HCV: hepatitis C virus

HCVcc: HCV cell culture derived particles

MAVS: mitochondrial antiviral signaling protein

MD: molecular dynamics

NMR: nuclear magnetic resonance spectroscopy

*N*N-DGJ: *N*-nonyl-deoxygalactonojirimycin

*N*N-DNJ: *N*-nonyl-deoxynojirimycin

NPHV: nonprimate hepacivirus

ORF: open reading frame

PI-IRES: poliovirus internal ribosomal entry site

RT: room temperature

SP: signal peptide

TM1/2: transmembrane helix 1/2

TRIF: Toll-IL-1 receptor domain-containing adaptor inducing interferon-beta

UTR: untranslated regions

Abstract

Nonprimate hepacivirus (NPHV), the closest homolog of hepatitis C virus (HCV) described to date, has recently been discovered in horses. Even though both viruses share a similar genomic organization, conservation of the encoded hepaciviral proteins remains undetermined. The HCV p7 protein is localized within endoplasmic reticulum (ER) membranes and is important for production of infectious particles. In this study, we analyzed the structural and functional features of NPHV p7 in addition to its role during virus assembly. Three-dimensional homology models for NPHV p7 by using various NMR structures were generated highlighting conserved residues important for ion-channel function. By applying a liposome permeability assay, we observed that NPHV p7 exhibited similar liposome permeability features than HCV p7 indicative of similar ion-channel activity. Next, we characterized the viral protein using a p7-based *trans*-complementation approach. A similar sub-cellular localization pattern at the ER membrane was observed, although production of infectious particles was likely hindered by genetic incompatibilities with HCV proteins. To further characterize these cross-species constraints, chimeric viruses were constructed by substituting different regions of HCV p7 with NPHV p7. The N-terminus and transmembrane domains were non-exchangeable and therefore constitute a cross-species barrier in hepaciviral assembly. In contrast, the basic loop and the C-terminus of NPHV p7 were readily exchangeable allowing production of infectious *trans*-complemented viral particles. In conclusion, comparison of NPHV and HCV p7 revealed structural and functional homology of these proteins including liposome permeability and broadly acting determinants were identified which modulate hepaciviral virion assembly and contribute to the host-species barrier.

Importance

The recent discovery of new relatives of hepatitis C virus (HCV) enables for the first time the study of cross-species determinants shaping hepaciviral pathogenesis. Nonprimate hepacivirus (NPHV) was described to infect horses and represents so far the closest homolog of HCV. Both viruses encode the same viral proteins; however NPHV protein functions remain poorly understood. In this study, we aimed to dissect NPHV p7 on a structural and functional level. By using various NMR structures of HCV p7 as templates, three-dimensional homology models for NPHV p7 were generated highlighting conserved residues being important for ion-channel function. A p7-based *trans*-complementation approach and the construction of NPHV/HCV p7 chimeric viruses showed that the N-terminus and transmembrane domains were non-exchangeable. In contrast, the basic loop and the C-terminus of NPHV p7 were readily exchangeable allowing production of infectious viral particles. These results identify species-specific constraints as well as exchangeable contaminants in hepaciviral assembly.

Introduction

For more than two decades, hepatitis C virus (HCV) and GB virus B (GBV-B) were the sole members of the genus *Hepacivirus* within the *Flaviviridae* family. Recently, multiple new hepaciviruses have been identified in dogs (1), horses (2), bats (3, 4), rodents (3, 5), non-human primates (6), rats (7) and cattle (8, 9). Among them, nonprimate hepacivirus (NPHV), initially described to infect dogs and subsequently horses, is the closest homolog of HCV and thus represents a unique model to study differences in hepacivirus pathogenesis of HCV and HCV-related viruses (10, 11).

HCV is globally distributed and approximately 146 million people of the world's population are persistently infected (12). Individuals infected with HCV are at high risk of developing liver cirrhosis and hepatocellular carcinoma (13). The development of direct-acting antivirals (DAA's) has significantly improved antiviral treatment options (14). However, a prophylactic vaccine is still lacking. The genome of HCV consists of a single-stranded RNA with positive polarity and encodes for ten viral proteins in an open reading frame (ORF) (15). The small membrane protein p7 is encoded between the structural proteins core, E1 and E2 and the non-structural proteins. P7 is classified into the group of viroporins since it fulfills major characteristics of this family for instance its small size of 63 amino acids and its ability to form oligomeric, hydrophobic ion-channels in the endoplasmic reticulum (ER) membrane (16). P7 is composed of two transmembrane passages connected by a short polar loop. The N-terminal helix and C-terminus are facing towards the lumen of the ER (17), however another topology where the C-terminus is exposed towards the cytosol has also been reported (18). P7 monomers assemble to form hexameric or heptameric structures (19-22). By applying single-particle electron microscopy a three-dimensional model of a p7 hexamer was resolved (20). Additionally, the monomeric and oligomeric structure of p7 of different genotypes was elucidated by nuclear magnetic resonance

126 spectroscopy (NMR) studies in different lipid-mimicking environments (TFE, DHPC, DPC or
127 methanol) (23-26), which likely explains the structural discrepancies observed between these
128 models. *In vitro* analysis revealed that p7 is essential for HCV assembly and release, whereas it is
129 dispensable for viral replication (27, 28). For further details on structural and functional
130 properties of HCV p7 see also recent reviews (16, 29, 30).
131 After the identification of NPHV, several studies have been conducted to investigate differences
132 and similarities between NPHV and HCV. A high seroprevalence of anti-NPHV antibodies (30-
133 40%) among horses was reported with 2-7% of the horses also carrying viral RNA (10). Similar
134 to HCV, also NPHV is a hepatotropic virus as was evidenced by accumulation of viral plus and
135 minus strand RNA in liver sections (31). The genomic organization of HCV and NPHV is highly
136 conserved with one ORF encoding the viral proteins (10, 11). As seen for HCV, the ORF of
137 NPHV is flanked by two untranslated regions (UTR) at the 5' and 3' end with the 5'UTR
138 displaying a larger stem loop I (2). Regarding the function of NPHV viral proteins, individual
139 expression of the NPHV core protein showed that core localizes on lipid droplets as reported for
140 HCV core (32). In addition, the NS3/4A protein of NPHV has been shown to have a similar
141 function as the HCV equivalent by cleaving human mitochondrial antiviral signaling protein
142 (MAVS) and Toll-IL-1 receptor domain-containing adaptor inducing interferon-beta (TRIF) (33).
143 However, a detailed understanding of viral protein function especially in the context of cross-
144 species determinants shaping hepaciviral pathogenesis is lacking.
145 In this study, we discovered that although NPHV p7 shared comparable structural features with
146 its human homolog and exerted an ion-channel activity, the protein could not fully substitute
147 HCV p7 during virus assembly. Replacement of the basic loop and the C-terminus within NPHV
148 p7, however, led to production of infectious HCV particles, thus defining virus species-specific
149 and interchangeable subdomains within p7.

Materials and Methods

Sequence and phylogenetic analysis. Nucleotide sequences of NPHV p7 isolates (GenBank Accession numbers: KP325401, JQ434002, JQ434003, JQ434004, JQ434005, JQ434006, JQ434007, JQ434008, JX948116; generated p7 sequences of this study are available upon request) were translated and aligned using MEGA6 (34) and a consensus sequence was generated. For phylogenetic analysis one representative p7 sequence of each HCV genotype was utilized (GenBank Accession numbers: NC004102, YP001469630, NC009824, NC009825, NC009826, NC009827, EF108306). The HCV p7 consensus sequence was deduced from the ClustalW multiple alignment (35) of p7 sequences from representative HCV strains of confirmed genotypes (as described in reference (23)). A Maximum Likelihood phylogenetic tree was generated using MEGA6 (34).

Structural analysis. Three-dimensional homology models of NPHV p7 monomer were constructed by the Swiss-Model automated protein structure homology modeling server (http://www.expasy.org/spdbv/; (36)) by using the NMR structures of HCV p7 as templates (23-26). Two models of the NPHV p7 three-dimensional hexamer were generated. The positions of models 1 and 2 relatively to the membrane bilayer was deduced from molecular dynamics (MD) simulations of HCV p7 in POPC bilayer as reported in Chandler *et al.* (19) and Kalita *et al.* (37), respectively. Figures were generated from structure coordinates by using VMD (http://www.ks.uiuc.edu/Research/vmd/; (38)) and rendered with POV-Ray (http://www.povray.org/).

Peptide synthesis of HCV and NPHV p7. The p7 peptides of the JFH-1 or H14 strain were synthesized with a CEM microwave peptide synthesizer. Therefore, all required amino acids were

dissolved in N,-N,-dimethylformamide (DMF; Rathburn Chemicals Ltd). As activator hydroxybenzotriazole (HoBt) hydrate and as activator base N,N'-diisopropylcarbodiimide (DIC; Sigma) were used. Deprotection was conducted in 20% piperidine (Sigma) in DMF (v/v). Dichlormethane (Sigma) was used for washing. 16.4 l of DMF, 150 ml of activator, 200 ml of activator base, 2.8 l of deprotect, 0.17 g of resin and 0.2 M of each respective amino acid were placed in a CEM microwave peptide synthesizer and a programme was created to start synthesis from the C-terminus. The first amino acid added was arginine (Arg), since alanine (Ala) is attached to the resin. Reactions for all the amino acids were double coupling except proline. Cycles for Arg, Cys and His are performed at lower temperature and for a longer time period to avoid racemization. To avoid any side chain reaction only Fmoc-Lys (Boc)-OH for lysine (Lys) was used with double coupling. The instrument will automatically stop and collect the resin with synthesized peptide which is then required to cleave the peptide from resin. Peptides were purified by HPLC on a C4-semipreparative column with a linear acetonitrile gradient. The purity was verified by SDS PAGE. The sequence of the p7 peptide was confirmed by MALDI-TOF mass spectromic analysis.

Liposome permeability assay. Liposome preparation and permeability assays were conducted as described earlier (39). Briefly, lipids (Avanti Polar Lipids) in chloroform were added in a final mixture containing 0.5 mg L-α-phosphatidic acid, 0.5 mg L-α-phosphatidyl choline and 0.5 % w/w L-α-phosphatidyl ethanolamine with lissamine rhodamine B labelled head groups. Chloroform was evaporated from the lipids using a stream of nitrogen, before placing in a vacuum for 4 hours at room temperature (RT). Lipids were rehydrated to 2 mg/ml in a self-quenching concentration of carboxyfluorescein (CF) buffer (50 mM 5(6)-Carboxyfluorescein (SIGMA), 10 mM HEPES (pH 7.4), 107 mM NaCl) and vigorously shaken overnight at RT.

198 Unilamellar liposomes were produced using an extruder (Avanti Polar Lipids) and a 0.4 μm filter
199 (whatman). Liposomes were purified via centrifugation at 49 000 rpm for 15 min at 25°C
200 including 4 washing steps before the pellet was resuspended in 0.5 ml liposome assay buffer (10
201 mM HEPES, pH 7.4, 107 mM NaCl). For p7 activity assays the peptides were reconstituted in
202 100% DMSO and the concentration was determined by nanodrop. Liposomes supplemented with
203 1% v/v DMSO were used as a baseline for fluorescence. Assays were carried out in black-walled,
204 flat-bottomed black-base 96-well plates at 37°C. Each well contained 50 μM of liposomes
205 (calculated from the rhodamine fluorescence) and 1 μl of peptide in DMSO in a total volume of
206 100 μl with liposome assay buffer. 0.5 % v/v Triton TX-100, which lyses liposomes, was used
207 for gain adjustment, setting a level of 90% fluorescence. The 96-well plate was kept on ice for 2-
208 5 minutes after gain adjustment and while the peptide +/- drug was added. CF release measured
209 by increased fluorescence was taken as an indicator of peptide induced membrane permeability
210 (activity). A set of 30 readings (λ ex485/ λem520 nm) was made over the course of 24 minutes
211 using a FLUOstar Galaxy plate-reader (BMG Labtech). Each condition was carried out in
212 duplicate wells with three independent experimental repeats. End point measurements were used
213 for the analysis with the average of the duplicate wells taken. For NN-DNJ inhibition assays
214 liposomes contained 2% v/v DMSO +/- 40 μM NN-DNJ, these being the respective background
215 levels for drug-free and drug-treated wells. As peptide concentrations 9 μM of NPHV p7 peptide
216 and 44 μM of JFH-1 p7 peptide were used. Peptides +/- inhibitor were incubated for 20 minutes
217 at RT prior to addition to the gain adjusted plate on ice. Statistical analysis was conducted by a
218 Welch's corrected unpaired t-test. P-values <0.05 were considered as statistical significant (*).
219
220 **Cell culture.** Huh-7.5 cells were cultured in Dulbecco's modified Eagle's medium (Life
221 Technologies) supplemented with 10 % fetal bovine serum (FCS), 2 mM L-glutamine,

nonessential amino acids (Invitrogen), 100 µg/ml streptomycin (Invitrogen) and 100 IU/ml penicillin (Invitrogen) (DMEM complete) at 37°C and 5% CO2. The packaging cell line Huh-7.5[C][E1E2][NS2]J6 expressing the Jc1 derived proteins C, E1E2 and NS2 was generated by lentiviral gene transfer as described earlier (40). Vectors used for the gene transfer encoded for a blasticidin-S deaminase resistance gene and therefore 5 µg/ml of blasticidin (Invivogen) was added for selection.

Plasmids. The plasmids and pFK-PI-Spp7/J6-EI-NS3-5B/JFH-1, pFK-PI-Sp-HA-HA-L-p7/J6EI-NS3-5B/JFH-1 and pFK-PI-G-Luc-EI-NS3-5B/JFH-1 have been described earlier (41, 42) and are based on the bicistronic helper replicon pFK-PI-EI-NS3-5B/JFH-1. This helper replicon contains a poliovirus derived internal ribosomal entry site (IRES) (PI) downstream of the JFH-1 derived 5'-nontranslated region (5'NTR) (nucleotides 1 to 341 of JFH-1) and is separated by a spacer region of 72 nucleotides. The second cistron is under the control of an encephalomyocarditis virus IRES (EI) that expresses JFH-1 derived NS3 to NS5B proteins. The p7 sequence of the NPHV isolate H14 and different HCV/NPHV p7 chimeras were chemically synthesized (Integrated DNA Technologies, IDT). The cloned fragments included a signal peptide (sp) derived from the last 51 base pairs of the E2 protein (HCV isolate J6) downstream of the p7 sequence or additionally a HAHA-tag linked to the p7 sequence with a linker and upstream of the sp. The respective genes were cloned into the first cistron of pFK-PI-EI-NS3-5B/JFH-1 by restriction digest and ligation. In addition to bicistronic helper replicons used for trans-complementation assays, experiments with the HCV full length virus were also performed. Therefore the plasmids pFK-Jc1 (43), pFK-Jc1-Δp7half (27) and pFK-Jc1-HA-HA-L-p7/J6 (42) were utilized. The p7 sequence of the NPHV isolate H14 and the p7 sequences of HCV/NPHV chimeras (p7J6-loop-H14, p7J6-C-ter-H14 and p7J6-loop-C-ter-H14) were cloned into pFK-Jc1

246 and pFK-Jc1-HA-HA-L-p7/J6 by polymerase chain reaction (PCR)-based insertion. All
247 constructs were confirmed by sequencing prior to use. Further details regarding the cloning
248 strategies and exact nucleotide sequences are available upon request.
249
250 ***In vitro* transcription and electroporation.** *In vitro* transcripts were created according to the
251 protocol described previously (40). DNA was purified by the Qiaquick PCR purification kit
252 (Qiagen) and RNA was purified by the NucleoSpin RNA Extraction Kit (Macherey Nagel)
253 according to the manufacturer's instructions. Concentration was determined by nanodrop. *In vitro*
254 transcribed RNA was stored at -80°C until electroporation.
255 Electroporations were conducted as described earlier (40). Briefly, Huh-7.5 or Huh-
256 7.5[C][E1E2][NS2]J6 cells were trypsinized, taken up in DMEM complete and the cell number
257 was determined. A final concentration of $1.5x10^7$ cells/ml in 400 µl of Cytomix (120 mM KCl,
258 0.15 mM $CaCl_2$, 10 mM K_2HPO_4/KH_2PO_4 (pH 7.6), 25 mM HEPES, 2 mM EGTA, 5 mM
259 $MgCl_2$, adjust pH to 7.6 with KOH) supplemented with 2 mM ATP and 5 mM Glutathione per
260 electroporation and 5-10 µg of *in vitro* transcripts were used per electroporation. Transfected
261 cells were directly taken up in 12-16 ml DMEM complete and seeded into 6-well plates or 10 cm
262 dishes depending on the application.
263
264 **Immunofluorescence.** After transfection, cells were seeded into a 24-well plate onto coverslips.
265 Cells were fixed 48 h post transfection by addition of 3% paraformaldehyde. Staining of
266 intracellular HAHA-tagged p7 and a co-staining of E2 or NS3 was performed as described
267 elsewhere (42). In brief, fixed cells were permeabilized with 0.5% Triton-X100 for 10 minutes at
268 RT. Blocking was conducted for one hour at RT in blocking buffer (5% goat serum (Sigma) in
269 PBS). The primary antibodies were incubated overnight at room temperature in blocking buffer.

The primary mouse α-HA antibody (Covance) was diluted 1:1000, the primary rabbit α-NS3 4949 (44) was diluted 1:400 and the primary human α-E2 antibody CBH-23 (45) was diluted 1:250 in blocking buffer. The α-NS3 and α-E2 antibodies were kind gifts from R. Bartenschlager (University of Heidelberg) and S. Foung (Stanford University), respectively. Species-specific secondary antibodies (A488-conjugated α-mouse IgG, A546-conjugated α-rabbit IgG and A546-conjugated α-human IgG) were diluted 1:1000 in blocking buffer and incubated for 1 hour at RT in the dark. Cell nuclei were stained with DAPI (Invitrogen). Last, coverslips were mounted on glass slides using Fluoromount-G (Southern Biotech). Pictures were taken using a x100 magnification lens by an inverted confocal laser-scanning microscope (Olympus Fluoview 1000). A sequential acquisition mode with an average of 3 frames for each picture (Kalman n=3) was applied for the 3 channels used.

Western blot. Western blot analysis of cell lysates was performed as previously described (42). Briefly, cells were lysed 48 h post transfection by addition of 1% Trition-X100 supplemented with protease inhibitor (Roche). Nuclei were separated by centrifugation and reducing sample buffer was added to the supernatant. Samples were incubated at 37°C for 15 minutes prior separation by SDS-PAGE. After transfer of the separated proteins on a membrane, the membrane was incubated for 1 h in blocking solution (5% milk in 0.05% Tween/PBS). The primary antibody was incubated over night at 4°C in blocking solution. The following dilutions were used for the antibodies: mouse α-HA (Sigma) 1:1000; mouse α-NS5A 9E10 (46) 1:1000; mouse α-NS2 6H6 (47) 1:1000; mouse α-E2 AP33 1:1000; mouse α-βactin (Sigma) 1:1000. The α-NS5A 9E10 and α-NS2 6H6 antibodies were a generous gift from C. M. Rice (Rockefeller University). The α-E2 AP33 antibody was provided by Genentech and Arvind Partel (University of Glasgow) (48). The secondary horseradish peroxidase-conjugated (HRP)-coupled antibody (α-mouse,

294 Sigma) was incubated for 1 h at room temperature. It was diluted 1:20 000 except after
295 incubation with the α-HA antibody (1:2000). After washing in 0.05% Tween/PBS,
296 chemiluminescence was obtained with the ECL Plus Western Blotting Detection System (GE
297 Healthcare) and measured using a ChemoCam Imager.
298
299 **Virus titration.** To determine viral titers in collected supernatants, a limiting dilution assay was
300 conducted on Huh-7.5 cells. The 50% tissue culture infectious dose ($TCID_{50}$) was determined 72
301 h post infection as reported earlier (40).
302

Results

NPHV p7 amino acid sequence is highly conserved and shows structural features comparable to HCV p7

To examine the degree of p7 amino acid sequence conservation among different NPHV p7 isolates, 15 distinct NPHV p7 sequences were aligned and a consensus sequence was generated (Fig. 1A). The identification of the respective NPHV p7 sequences was based on cleavage site predictions as reported earlier (11). Overall, the NPHV p7 sequences were highly conserved at the amino acid level with only 11 positions (over the 63 residues) showing some variations (Fig. 1A). Alignment of globally sampled NPHV and HCV p7 nucleotide sequences and subsequent phylogenetic analysis revealed a high level of divergence between HCV and NPHV, with each virus forming a discrete, well supported clade (Fig. 1B). Of note, sampled NPHV p7 isolates showed a remarkably lower nucleotide variation when compared to HCV p7 isolates derived from genotypes (GT) 1-7, which is indicated by the different branch lengths (Fig. 1B). Database searching for proteins related to NPHV p7 using either Blast (49) or Fasta (50) revealed that p7 from HCV genotype 4f displays the highest similarity to the NPHV consensus sequence, with 33% of identical amino acids and 28% and 13% of strongly and weakly similar amino acids. Moreover, similar percentages were observed when comparing the NPHV p7 consensus sequence with p7 consensus sequences from representative HCV strains of confirmed genotypes (51, 52) (19% identical, 24% strongly similar, 16% weakly similar and 30% different residues; Fig. 2A). With respect to the non-conserved residues, one can distinguish those exhibiting obvious physicochemical differences (colored dark blue in Fig. 2A) from those for which the hydrophobic or hydrophilic character is conserved (colored light blue). Moreover, most of the latter NPHV p7 residues could be observed as minor variants in the p7 amino acid repertoire of HCV reference genotypes (reported in Fig. 2A in (27); residue positions 11, 22, 37, 44, 45 and 51). In total, only

20% of residue positions distributed along the sequence appeared to be clearly specific for NPHV and HCV p7, including positions 1, 5, 7, 9, 13, 14, 16, 29, 33, 39, 43, 46 and 47. Altogether, these data indicate that the overall structure of NPHV p7 should be comparable to that of HCV p7. This was also supported by secondary structure analyses and predictions of transmembrane segments, which exhibited similar patterns for NPHV and HCV p7 (data not shown).

Several NMR structures have been reported for HCV p7 (19, 23-26) allowing us to construct three-dimensional homology structure models for NPHV p7 by using the Swiss-Model automated protein structure homology modeling server (http://www.expasy.org/spdbv/; (36)) and the consensus NPHV p7 sequence as input. The four resulting homology structure models for the monomeric form of NPHV p7 are depicted in Figure 2B. The three first models exhibited a "hairpin-like" topology consisting of two transmembrane segments that are connected by a hydrophilic, positively charged cytosolic loop containing residues 33 and 35. According to the corresponding hexameric forms of these models (19, 24, 25) and to the typical oligomeric structure of viroporins (53), NPHV p7 subunits would reside side-by-side as illustrated by model 1 in Figure 2C. In contrast, NPHV p7 homology model based on the NMR structure of hexameric p7 reported by Ouyang *et al.* (26) would exhibit an unusual architecture where part of each p7 subunit crosses over to interact with other p7 subunits that are not its neighbors (model 2, Fig. 2C). Nevertheless, these models allowed the positioning of conserved, very similar, similar, different and very different residues (colored from red to blue, respectively) along the secondary structure elements for each model (Fig. 2B) as well as at the surface of hexamer models and within their ion-channel pores (Fig. 2C).

NPHV p7 exerts an ion-channel activity in a liposome permeability assay

As the NPHV p7 structural analyses revealed similar features to HCV p7, we next used the liposome permeability assay previously reported for HCV p7 (39) to evaluate its ion-channel features. To produce the respective p7 peptides of NPHV (isolate H14) and HCV (isolate JFH-1), a chemical synthesis was performed (see Material and Methods). The p7 peptides were reconstituted in DMSO and validated using mass spectrometry and SDS-PAGE, before increasing doses of the peptides were incubated with liposomes previously loaded with carboxyfluorescein (CF) at self-quenching concentrations . In this assay, increase in membrane permeability was measured by the dye release and dequenching. An increase of fluorescence was observed when the NPHV p7 peptide was added to the liposomes, which reached a plateau with a peptide concentration of 10-20 μM (Fig. 3A). The HCV JFH-1-derived peptide demonstrated an ion-channel activity in a dose-dependent manner with about 2-3-fold higher fluorescent units (FU) compared to NPHV p7 (Fig. 3B). As the iminosugar derivative *N*-nonyl-deoxynojirimycin (*N*N-DNJ) was reported to block the HCV p7 ion-channel activity (54), we analyzed the inhibitory effect of *N*N-DNJ against NPHV p7. As depicted in Figure 3C, NPHV p7-dependent permeabilization of liposomes could be blocked with 40 μM *N*N-DNJ in a similar fashion as HCV p7 (Fig. 3C). Taken together, similar to HCV p7, these data indicate that NPHV p7 is likely able to exert an ion-channel function which can be blocked by iminosugar derivatives.

Cross-species substitutions of the basic loop and the C-terminus in p7 lead to production of *trans*-complemented particles

To study the capability of NPHV p7 to rescue production of infectious particles, we made use of a p7-based HCV *trans*-complementation system (41). This system permits the evaluation of p7 function in virus-producing cells independently of secondary effects on polyprotein processing. The p7 sequence originating from the NPHV isolate H14 was cloned into the first cistron of a

374 bicistronic JFH-1 helper replicon (Fig. 4A). The p7 sequence was located downstream of a signal
375 peptide (sp) sequence encompassed within the last 51 amino acids of the HCV E2 protein derived
376 from the J6 isolate. Additionally and to facilitate p7 detection, another construct containing a sp,
377 HAHA-tag and a short linker sequence (GGGGSG) connected to NPHV p7 H14 was created. The
378 analogous constructs containing HCV p7 of the isolate J6 or the *Gaussia*-Luciferase gene (G-
379 Luc), both previously described (41, 42), were utilized as positive and negative controls,
380 respectively. The second cistron encoded for the non-structural proteins NS3-NS5B from the
381 HCV isolate JFH-1. *In vitro* transcripts of these constructs were individually transfected into a
382 packaging cell line encoding for the remaining viral proteins, core (C), E1E2 and NS2 from the
383 HCV isolates J6 and JFH-1 (Fig. 4A). To confirm the expression of HAHA-tagged p7, we
384 performed Western blot analysis showing that both HAHA-tagged p7 J6 and HAHA-tagged p7
385 H14 were expressed (Fig. 4B). However, in the lysate of HAHA-tagged p7 H14 additional
386 proteins with a higher molecular weight were detected (Fig. 4B) indicating SDS-resistant
387 oligomeric forms of the HAHA-tagged p7. Next, we analyzed the sub-cellular localization of
388 HAHA-tagged p7 in fixed cells by indirect fluorescence microscopy using antibodies recognizing
389 the HA-tag, HCV NS3 or E2 proteins in order to permit the assessment of co-localization
390 between these polypeptides (Fig. 4C). Both HAHA-tagged p7 proteins, J6 and H14, showed a
391 similar localization in the cytoplasm at ER membranes by co-localizing with E2 and NS3. The
392 rescue of HCV particle production by NPHV p7 was assessed after transfection of the packaging
393 cell line with the different p7 variants and infectivity released into the cell culture supernatant of
394 transfected cells. The J6-derived p7 construct could be rescued with peak titers of $5x10^4$
395 $TCID_{50}$/ml, while the double HA-tagged genome produced lower viral progeny as previously
396 reported (42). In contrast, NPHV p7 (with or without epitope tag) could not substitute the HCV

p7 function in this *trans*-complementation setting suggesting genetic incompatibilities between NPHV p7 and HCV proteins.

To explore if NPHV p7 and HCV p7 contain virus-specific but potentially also interchangeable (thus functionally conserved) subdomains, we replaced parts of HCV p7 with sequences of NPHV p7. To this end, we constructed eleven distinct chimeras by dividing p7 into the N-terminal, transmembrane helix 1 (TM1), basic loop, transmembrane helix 2 (TM2) and C-terminal subdomain (Fig. 5A). All chimeric constructs were N-terminally tagged with a double HA-tag connected by a short linker and preceded by a signal peptide sequence. These sequences were cloned into the first cistron of a bicistronic JFH-1 helper replicon and *in vitro* transcripts were transfected into Huh-7.5[C][E1E2][NS2]J6 packaging cells analogous to Figure 4A. Expression of HAHA-tagged p7 variants was assessed by immunofluorescence analysis showing the expression of chimeras 1, 2, 3, 5 and 11 and low or undetectable expression for the remaining constructs (Fig. 5B) indicating an early degradation or a general incompatibility between HCV p7 and NPHV p7 parts. Next, we investigated the capability of these p7 chimeras to *trans*-complement the production of infectious particles. The p7 chimeras 3 (replacement of the loop, subsequently termed p7J6-loop-H14), 5 (replacement of the C-terminus, subsequently termed p7J6-C-ter-H14) and 11 (replacement of the loop and C-terminus, subsequently termed p7J6-loop-C-ter-H14) were able to produce infectious particles (Fig. 5C). Viral titers of about 1-2 orders of magnitude lower compared to p7J6 were observed with p7J6-C-ter-H14 showing the highest titers. Replacement of the loop decreased the viral titers about 50-fold more drastically and delayed the virus kinetics. To further examine the functionality of these chimeras, the bicistronic replicons encoding for p7J6, p7H14, p7J6-loop-H14, p7J6-C-ter-H14 and p7J6-loop-C-ter-H14 N-terminally linked to a signal peptide were co-transfected into Huh-7.5 cells with Jc1Δp7$_{half}$, a HCV full length mutant described to completely abrogate viral particle production

421 (27) (Fig. 5D). As shown in Figure 5E, p7J6 as well as p7J6-loop-H14, p7J6-C-ter-H14 and p7J6-
422 loop-C-ter-H14 were able to rescue infectious particle production (Fig. 5E). In conclusion, cross-
423 species determinants in the basic loop and the C-terminus of hepaciviral p7 could be identified by
424 using a p7-based *trans*-complementation system.
425
426 **Cross-species determinants of NPHV p7 are important in late steps of the viral life cycle**
427 After the identification of cross-species determinants in hepaciviral virion production by creating
428 HCV/NPHV p7 chimeras, we next validated their functionality in the context of full-length HCV
429 cell culture derived particles (HCVcc). Hence, we cloned p7J6-loop-H14, p7J6-C-ter-H14, p7J6-
430 loop-C-ter-H14 and p7H14 into Jc1 and Jc1 HAHA-L-p7 (Fig. 6A). As positive control we
431 included the HCV constructs Jc1 and Jc1 HAHA-L-p7J6. These genomes were transfected into
432 Huh-7.5 cells and expression of epitope-tagged p7 was visualized 48 h later by Western blot
433 analysis. For the positive control Jc1 HAHA-L-p7J6 HAHA-tagged p7 could be detected as well
434 as the precursor proteins p7-NS2 and E2-p7-NS2 (Fig. 6B). In case of HAHA-L-p7H14 cleavage
435 defects were noted with signals at a molecular weight of approximately 24 kDa and 50 kDa
436 suggesting processing defects due to the insertion of H14 p7 into Jc1 (Fig. 4B). These proteins
437 were also detected for p7J6-loop-H14 and p7J6-loop-C-ter-H14, but here also free p7 was visible.
438 The p7J6-C-ter-H14 chimera showed an HA-detection pattern like the parental construct (Fig.
439 6B) indicating processing defects possibly at the E2/p7 junction or different oligomerization
440 forms. In addition, Western blot analysis to visualize NS2 and E2 in the same cell lysates was
441 conducted showing that only the precursor p7NS2 and no free NS2 can be detected for Jc1
442 HAHA-L-p7H14 (Fig. 6C).
443 Next, the release of infectious viral particles for the Jc1 constructs (Fig. 6D) and Jc1 HAHA-L-p7
444 (data not shown) constructs was determined by $TCID_{50}$ at different time points post transfection.

All HCV/NPHV epitope-tagged p7 chimeras led to the production of infectious particles while displaying delayed time kinetics and lower titers compared to Jc1 HAHA-L-p7J6 (data not shown). Moreover, as reported previously (42), these titers were around one order of magnitude lower compared to the untagged constructs shown in Figure 6D. Jc1 p7J6-loop-C-ter-H14 showed the lowest production of infectious particles, whereas Jc1 p7H14 was not able to produce infectious particles, which is in concordance to the results in the *trans*-complementation system. As HCV p7 was reported to be important for the assembly and release step of the viral life cycle (27, 28, 41), we investigated whether this function was also conserved in the context of the p7 chimeric genomes. To this end, we determined extra- and intracellular core amounts 48 h post transfection (Fig. 6E) and calculated the specific infectivity for each construct (Fig. 6F). The intracellular core amounts were comparable for all constructs, whereas the recombinant chimeric constructs displayed a reduction in extracellular levels of core with Jc1 p7H14 at background levels in line with the results from the infection assay (Fig. 6E). Therefore, the specific infectivity of Jc1 p7J6-loop-H14 and Jc1 p7J6-C-ter-H14 was comparable to Jc1 demonstrating an importance of NPHV p7 in viral assembly and release of infectious particles rather than in virus entry. In case of the Jc1 p7J6-loop-C-ter-H14 the infectivity levels and extracellular core amounts were minimal, therefore no specific infectivity could be calculated. Taken together, HCV/NPHV p7 chimeras defining cross-species determinants of virion assembly were functional in the context of HCV cell culture particles and were crucial for the late steps of the viral life cycle.

Virion production of HCV/NPHV p7 chimeras can be inhibited by prototypic ion-channel blockers

Inhibitors including rimantadine and iminosugar derivatives blocking the ion-channel function or oligomerization of HCV p7 have been described (55), but their detailed mechanism of action is

not well defined. To facilitate the understanding of p7 inhibitor functions and evaluate the ion-channel activity of the HCV/NPHV p7 chimeras in the context of the complete viral life cycle, we next tested the antiviral activity of the prototypic ion-channel inhibitors rimantadine (Fig. 7A) and two iminosugars *N*-nonyl-deoxygalactonojirimycin (*N*N-DGJ) (Fig. 7B) and *N*-nonyl-deoxynojirimycin (*N*N-DNJ) (Fig. 7C) against Jc1 p7J6-loop-H14 and Jc1 p7J6-C-ter-H14. Inhibitors were added to cells 4 h post transfection and viral titers were determined 48 h post transfection. Jc1 p7J6-loop-H14 was inhibited by rimantadine, *N*N-DGJ and *N*N-DGJ to a similar level as the Jc1 wildtype (Fig. 7A, B and C). In contrast, Jc1 p7J6-C-ter-H14 showed a slightly higher resistance profile to rimantadine and *N*N-DGJ compared to the parental Jc1 construct (Fig. 7A and B) indicating a lower binding affinity and less inhibitory activity of these inhibitors when structural changes occur at the C-terminus of p7. These results indicate that in the context of HCV/NPHV p7 chimeric viruses functional ion-channels are formed which can be inhibited by specific p7 inhibitors.

Discussion

In this study, we performed a comparison of NPHV and HCV p7 on a structural and functional level. Sequence alignment of reported and novel p7 isolates revealed a high level of conservation among all isolates, especially when compared to the variation apparent among HCV isolates. This is in accordance with the overall high conservation of the full NPHV genome between different isolates, where a diversity of approximately 15% was reported in contrast to 30% of diversity between HCV isolates (10). Amino acid sequence similarities indicate that the overall structure of NPHV p7 is comparable to that of HCV p7, allowing us to construct NPHV p7 homology models using reported three-dimensional NMR-based HCV p7 structures (19, 23-26) as templates for monomeric and hexameric models. A greater degree of amino acid identity was found in the C-terminal 48-63 p7 segment, including conservation of the upstream cleavage site of the signal peptidase at the p7-NS2 junction. Despite the amino acid variability in 37-47 segment when compared to HCV p7, the overall C-terminal half of p7 NPHV exhibits the characteristic structural features of a signal peptide (Fig. 2A), and thus likely acts as a signal for the re-initialization of translocation of the C-terminal part of p7. Interestingly, most of the different residues in this segment are located at the surface of the hexamer homology models, and thus should not disturb ion-channeling function of p7, but could potentially play a role in p7 interactions with other viral or cellular partners. Additionally, a high degree of amino acid similarity was found in segment 17-32, which is thought to be the main structural element involved in p7 pore formation and function. An interesting difference is the presence of only one basic residue at position 35 in the putative cytosolic loop of NPHV p7 instead of two fully conserved basic residues at positions 33 and 35 in p7 of all HCV genotypes (17). This suggests that the basic residue at position 33 in HCV might be not essential for p7 functioning. Moreover, the N-terminal segment 1-16 exhibited lower similarity with several different residues located

both at the surface of the hexamer models or facing the pore lumen. These features suggest that this relatively poorly homologous segment should not play a critical role in ion-channeling but could be important for specific interactions with other viral and/or host-specific cellular factors. Moreover, as observed in HCV p7, this N-terminal segment also might play an essential role in the complex mechanism of E2-p7 processing by signal peptidase (56, 57). Together, all these structural features indicate a possible ion-channel function of NPHV p7 similar to HCV p7, which is supported by the results of the liposome permeability assay. For chemically synthesized p7 peptides of NPHV and HCV an increase of CF release with a concurrent increase of the peptide concentration was observed. However, due to the property of the NPHV p7 peptide to form aggregates at high concentrations, the effect was observed at lower peptide concentrations and at an early peak compared to the HCV p7 peptide. The observed CF release could be blocked by addition of the iminosugar *N*N-DNJ indicating an ion-channel function of NPHV p7. The dibasic motif K33-R35 of HCV p7 was reported earlier to be important to maintain the ion-channel activity in liposomes (58). Importantly and in line with the structural analysis of NPHV p7, only the basic residue at position 35 is conserved in NPHV p7 and not the basic residue at position 33, leading to the assumption that specifically residue 35 is essential to preserve p7 function.

We next investigated NPHV p7 determinants specific to NPHV or conserved between HCV and NPHV. Moreover, we analyzed its sub-cellular localization and its role in the viral life cycle. By using a p7-based *trans*-complementation approach, which is independent of viral polyprotein processing, we could show that NPHV p7 was successfully expressed despite the detection of oligomeric forms of NPHV p7. These oligomeric intermediates have not been observed for HCV p7 so far. Nevertheless, the successful expression of NPHV p7 allowed us to investigate the sub-cellular localization in infected cells. The highest degree of co-localization of HCV p7 with viral

proteins has been described for E2, whereas also co-localization with NS2, NS3, NS5A and in parts core were reported (42). This is in accordance with our localization analysis showing that epitope tagged NPHV p7 co-localizes with NS3 and E2 in a similar pattern as epitope tagged HCV p7 in the cytoplasm of the cell. Despite the expression of NPHV p7 and sub-cellular localization similar to HCV p7, no infectious particles were produced in the *trans*-complementation system probably due to genetic incompatibilities of viral proteins. We could demonstrate previously that even the replacement of genotype 2a J6-p7 by another HCV isolate Con1 (genotype 1b) fully abrogated HCV particle production and even replacement by p7 of another genotype 2a isolate (JFH-1) did significantly reduce the release of infectious particles (27, 41). To overcome these cross-species genetic incompatibilities, HCV/NPHV p7 chimeras were constructed demonstrating that the basic cytosolic loop and C-terminus of NPHV p7 as well as the combination of both are interchangeable between NPHV and HCV thus restoring HCV infectious particle production. For HCV, inter-genotypic p7 chimeras were also analyzed for being infectious *in vivo* when the N-terminal and C-terminal tails of p7 from a genotype 1a virus were maintained, but other parts substituted by genotype 2a sequences (59). Moreover, we observed that the basic loop could be substituted without abolishing particle formation underlying the importance of the basic residue 35 to maintain NPHV p7 functions. Lastly, we tested the generated chimeras as well as the full NPHV p7 sequence in an HCV full-length virus (HCVcc) revealing comparable virion production to the *trans*-complementation system that the complete NPHV p7 sequence could not compensate for HCV p7 function due to cross-species incompatibilities. In addition, Western blot analysis showed an absence of mature NPHV p7 with the correct molecular weight. However, the detected proteins coincide with the molecular weight of the proteins detected in the *trans*-complementation system, where no precursor proteins are produced indicating an oligomerization of NPHV p7 rather than a cleavage defect. Nevertheless,

555 the novel chimeras were fully functional and were shown to be important for viral assembly and
556 release. Thus, virus-specific determinants of hepaciviral virion assembly are located in the N-
557 terminus and transmembrane regions of p7.
558 Inhibitor experiments with rimantadine and the iminosugar derivatives *N*N-DGJ and *N*N-DNJ
559 were conducted since these prototypic ion-channel inhibitors were reported to target HCV p7 and
560 reduce particle production (60). These experiments showed that the HCV/NPHV p7 chimera
561 carrying the C-terminus of NPHV p7 was more resistant especially to rimantadine and *N*N-DGJ
562 at high concentrations. The interaction sites of rimantadine with HCV p7 were analyzed
563 previously (24) showing key interacting residues at position 46, 48 and 52, which are present in
564 the chimeric construct. However, the change of the C-terminus of p7 could influence the overall
565 p7 folding, which could compress the rimantadine binding cavity leading to a less favourable fit
566 for the molecule resulting in a more drug-resistant phenotype. The iminosugar derivative *N*N-
567 DNJ demonstrated an inhibition of all viruses at the highest concentration, which may results not
568 only from the p7 ion-channel inhibition, but also from the blockage of ER α-glucosidases
569 required for folding and maturation of the HCV glycoproteins (60).
570 In conclusion, the identification of viruses closely related to HCV allowed for the first time a
571 cross-species comparison of two naturally occurring hepaciviral species. We could show that the
572 overall structure of NPHV p7 is highly conserved compared to HCV p7 and that NPHV p7 most
573 likely exhibits an ion-channel activity. Molecular analysis revealed a similar sub-cellular
574 localization of NPHV p7 with an ER-like pattern. Moreover, although NPHV p7 could not fully
575 replace HCV p7 function, the basic loop and C-terminus could be substituted leading to the
576 production of infectious particles. The results implicate a similar role of NPHV p7 in viral
577 pathogenesis as seen for its human homolog and identify broad hepaciviral protein determinants
578 for virus assembly.

579
580

581 **Figure legends**

582 **Figure 1**

583 **Sequence and phylogenetic analysis of NPHV p7.** A) Amino acid conservation in NPHV p7.
584 Top panel represents a sequence logo (61) of the 63 amino acid NPHV p7 ion-channel generated
585 from an alignment of 15 globally sampled strains (GenBank Accession numbers: KP325401,
586 JQ434002, JQ434003, JQ434004, JQ434005, JQ434006, JQ434007, JQ434008, JX948116;
587 generated p7 sequences of this study are available upon request). Nucleotide sequences were
588 translated and aligned using MEGA6 (34). Individual amino acids are color-coded according to
589 physiochemical properties and individual residue frequencies in the population are proportional
590 to the x-axis. The global NPHV p7 consensus sequence is positioned directly below with *
591 indicating complete conservation at the amino acid level in all sampled strains. B) Phylogenetic
592 comparison of NPHV and HCV p7. NPHV and HCV p7 nucleotide sequences (189 bp) were
593 aligned and a Maximum Likelihood phylogenetic tree generated using MEGA6 (34). NPHV p7
594 sequences represent all available reported sequences downloaded from GenBank, in addition to
595 sequences generated in this study (GenBank Accession numbers: KP325401, JQ434002,
596 JQ434003, JQ434004, JQ434005, JQ434006, JQ434007, JQ434008, JX948116, H10, H14-H18).
597 HCV p7 sequences represent a single isolate from genotypes (GT) 1-7 (GenBank Accession
598 numbers: NC004102, YP001469630, NC009824, NC009825, NC009826, NC009827,
599 EF108306). Branch lengths are proportional to the scale bar and equivalent to genetic distance
600 measured in nucleotide substitutions per site.

601

602 **Figure 2**

603 **Homology structure models of NPHV p7.** A) Comparison of the NPHV p7 consensus sequence
604 (see also Fig. 1) to HCV p7 consensus sequence. The degree of amino acid physicochemical

conservation at each position is inferred with the similarity index according to ClustalW convention (asterix, invariant, red; colon, highly similar, dark pink; dot, similar, pink). Non-conserved but slightly different residues are colored light blue, while very different residues are colored dark blue. Underlined residues correspond to positions exhibiting conserved aromatic residues. Positions 33 and 35 in the central cytosolic loop are boxed. Note that the C-terminal half part of p7 exhibits structural features that are characteristic of signal peptides (62), consisting of an N-terminal region (n-domain) encompassing 1–3 positively charged residues (Arg), a hydrophobic core region (h-domain) forming an alpha-helix, and a more polar, flexible region (c-domain) containing a signal peptidase cleavage site; residues at positions -1 and -3 relative to the cleavage site are small neutral residues (Ala) and form the recognition site for signal peptidases (63), whereas alpha-helix-destabilizing residues (Pro, Gly) are present at position -6 and/or in the middle of the h-domain. B) Ribbon representation of the three-dimensional homology models of NPHV p7 monomer. Four previously published NMR-based structures were used as templates for modeling (23-26). Left, p7 monomer structure determined by NMR in 50% TFE and molecular dynamic (MD) simulations ((23); PDB entry); middle left, NMR-based structure of p7 monomer determined in 125 mM DHPC ((25); PDB entry, 2MTS); middle right, Flag-p7 monomer structure determined in 100% MeOH ((24); PDB entry, 3ZD0; the Flag tag and C-terminal extension are not shown); right, one subunit of hexamer p7 NMR structure model determined in 200 mM DPC ((26); PDB entry, 2M6X). N- and C-termini are noted by “N” and “C”, respectively. Alpha-helical segments are indicated and residues are color-coded according to panel A. Residues 33 and 35 side-chain atoms are represented as van der Walls spheres and illustrate the location of the central cytosolic loop of p7. C) Three-dimensional homology models 1 and 2 of NPHV p7 hexamer using the HCV p7 NMR/MD model in POPC of Chandler *et al.* ((19); model 1) and the HCV p7 NMR model in DPC of Ouyang *et al.* ((26); model 2) as

templates. Two opposing subunits are shown in the left. Hexameric forms of NPHV p7 models are in surface representations from different viewpoints: middle left, side view of the hexamer surface; middle right, sectional view showing the pore interior with its axis symbolized by the dashed line; right, ER lumen view showing the pore. Residues are color-coded according to panel A and B. Thick green lines shown in the left hand panels represent the polar membrane bilayer interfaces and hydrophobic core (between the middle two lines).

Figure 3

Evaluation of the NPHV p7 ion-channel activity in a liposome permeability assay. The HCV and NPHV p7 peptides were chemically synthesized and used for subsequent liposome permeability assays. P7 peptides originating from the A) NPHV isolate H14 and B) HCV isolate JFH-1 were reconstituted in DMSO. Different concentrations of peptide were added to 50 µM of carboxyfluorescein loaded liposomes and the fluorescence units [FU] were measured as an indicator of peptide-induced membrane permeability (activity). Liposomes supplemented with 1% v/v DMSO were used as solvent control. Three independent experiments in duplicate wells were conducted and mean values +/- SD are depicted. C) Inhibition assays with *N*N-DNJ were conducted. Therefore, liposomes contained 2% v/v DMSO +/- 40 µM *N*N-DNJ, these being the respective background levels for drug-free and drug-treated wells. As peptide concentrations 9 µM of NPHV p7 peptide and 44 µM of JFH-1 p7 peptide were used. Peptides +/- inhibitor were incubated for 20 minutes at RT prior to addition to the gain adjusted plate on ice. Three independent experiments in duplicate wells were conducted. Depicted is the mean value +SD normalized to the respective solvent control. The percentage of inhibition was calculated by normalizing to the DMSO control without inhibitor. Statistical analysis was conducted by a Welch's corrected unpaired t-test. P-values <0.05 were considered as statistical significant (*).

Figure 4

Analysis of NPHV p7 in a *trans*-complementation setup. A) Experimental setup. The p7 sequence of the HCV isolate J6 and of the NPHV isolate H14 (sequence available upon request) were cloned either untagged or linked to a HAHA-tag into the first cistron of a bicistronic helper replicon as previously reported (42). The signal peptide-coding sequence (sp) corresponded to the last 51 base pairs from the E2 J6 sequence was cloned downstream of p7. The insertion of a *Gaussia* luciferase (G-Luc) served as a negative control. The second cistron encodes for the non-structural proteins NS3-NS5B originating from the HCV isolate JFH-1. These bicistronic helper replicons were individually transfected into a packaging cell line expressing the remaining viral proteins core (C), E1E2 and NS2 from the HCV isolate J6. B) The expression of HAHA-tagged p7 in cell lysates was confirmed 48 h post transfection by Western blot analysis. Additionally, the viral protein NS5A and a cellular protein β-actin were stained. C) Co-staining of NS3 and HAHA-tagged p7 (upper panel) and of E2 and HAHA-tagged p7 (lower panel) was performed 48 h post transfection on fixed cells. Depicted in gray are single stainings with DAPI, α-HA, α-NS3 and α-E2 as well as a colored merge pictures. Here, cell nuclei are shown in blue, α-HA staining in green, and α-NS3 and α-E2 are shown in red, respectively. Pictures were taken using a 100x magnification lens. D) Viral titers in supernatants 24 h, 48 h and 72 h post transfection were determined by $TCID_{50}$. The mean of three independent experiments is depicted as $\log_{10}$ $TCID_{50}$/ml + standard deviation (SD).

Figure 5

Construction of HCV/NPHV p7 chimeras in a *trans*-complementation system. A) Eleven distinct HCV/NPHV p7 chimeras were constructed by dividing p7 into 5 parts (N-terminus,

677 transmembrane helix 1 (TM1), loop, transmembrane helix 2 (TM2) and C-terminus,
678 respectively). As templates the HCV isolate J6 and the NPHV isolate H14 were utilized and their
679 respective amino acid sequences are depicted. Amino acid sequences originating from H14 are
680 shown as light gray bars, whereas amino acids originating from J6 are shown as dark gray bars.
681 P7 chimeras were cloned into the bicistronic helper replicon including a signal peptide, a HAHA-
682 tag and a short linker according to Figure 4A. Constructed bicistronic helper replicons were
683 transfected into Huh7.5[C][E1E2][NS2]J6 by electroporation. B) Cells were fixed 48 h post
684 transfection and immunofluorescence analysis by staining for α-HA and DAPI was performed.
685 Shown are the respective merge pictures with the cell nuclei in blue and the α-HA staining in
686 green. Pictures were taken with a 100x magnification lens. D) Jc1 $\Delta p7^{half}$ was co-transfected into
687 Huh-7.5 cells with *in vitro* transcribed bicistronic JFH-1 helper replicons encoding for a signal
688 peptide (sp) downstream of p7J6, p7H14, p7J6-loop-H14, p7J6-C-ter-H14 and p7J6-loop-C-
689 terH14 in the first cistron as well as a G-Luc, respectively. E) Viral titers in supernatants 48 h
690 post transfection were determined by $TCID_{50}$ and the mean of three independent experiments is
691 depicted as $\log_{10}TCID_{50}$ +SD.
692
693 **Figure 6**
694 **Characterization of HCV/NPHV p7 chimeras in recombinant HCV cell culture viruses.** A)
695 The p7 sequence from the HCV isolate J6 and the NPHV isolate H14 as well as the designated
696 chimeras were cloned into Jc1 or Jc1 HAHA-L-p7 as depicted. B) *In vitro* transcripts of the Jc1
697 HAHA-L-p7 constructs as well as Jc1 wildtype were transfected into Huh-7.5 cells and the
698 expression of HAHA-tagged p7 in cell lysates was visualized by Western blot analysis 48 h post
699 transfection. Additionally, the viral protein NS5A and the cellular protein β-actin were stained.
700 C) Expression of NS2 and E2 in lysates of cells transfected with *in vitro* transcripts of the Jc1

HAHA-L-p7 constructs was visualized 48 h post transfection by Western blot analysis. D) Viral titers of the Jc1 p7 constructs were determined in supernatants 24 h, 48 h and 72 h after transfection into Huh-7.5 cells. Shown are $log_{10}TCID_{50}$/ml as mean values of three independent experiments + SD. E) Intra- and extracellular core amounts were measured 48 h post transfection of the Jc1 p7 constructs into Huh-7.5 cells. The background level of extracellular core amounts was set to the upper value of Jc1 p7H14, since this construct does not produce any infectious particles. Two independent experiments were performed and the mean values +SD as log_{10} core fmol/l are shown. F) The specific infectivity was calculated based on viral titers in panel C and extracellular core release in panel D.

Figure 7

Effect of p7 inhibitors on infectivity of HCV/NPHV p7 chimeras. *In vitro* transcripts of Jc1, Jc1 p7J6-loop-H14 and Jc1 p7J6-C-ter-H14 were electroporated into Huh-7.5 cells. 4 h post transfection the respective drug in two different concentrations or DMSO was added. Percentage of infectivity was calculated by determining the viral titer by $TCID_{50}$ and normalizing to the DMSO control. Three independent experiments were performed. Test of the inhibitory effect of A) Rimantadine (50 µM, 100 µM), B) *N*N-DGJ (5 µM, 50 µM) and C) *N*N-DNJ (5 µM, 50 µM].

Funding information

S. W. was supported by a stipend from the Helmholtz Centre for Infection Research and supported by Hannover Biomedical Research School (HBRS) and the Centre for Infection Biology (ZIB). E. S. was supported by the DFG (STE 1954/1-1) and intramural young investigator award of the Helmholtz Centre for Infection Research. A.K. and N.Z. are supported by the Oxford Glycobiology Institute. F.P. was supported by the Mapping project (ANR-11-BINF-003) and the French agency ANRS. T. P. was supported by a grant from the Helmholtz Association (SO-024) and by a grant from the European Research Council (ERC-2011-StG_281473-VIRAFRONT).

Acknowledgements

We are grateful to Takaji Wakita for gift of the JFH1 isolate, to Jens Bukh for the J6CF strain, to Charles Rice for Huh7.5 cells, the 9E10 and 6H6 monoclonal antibodies, to Ralf Bartenschlager for the NS3-specific antibody, to Steven Foung for the E2-specific antibodies and to Genentech and Arvind Patel for providing the AP33 antibody. We thank Daniel Todt for the statistical analysis and all members of the Institute of Experimental Virology, Twincore, for helpful suggestions and discussions.

References

1. **Kapoor A, Simmonds P, Gerold G, Qaisar N, Jain K, Henriquez JA, Firth C, Hirschberg DL, Rice CM, Shields S, Lipkin WI.** 2011. Characterization of a canine homolog of hepatitis C virus. Proceedings of the National Academy of Sciences of the United States of America **108:**11608-11613.
2. **Burbelo PD, Dubovi EJ, Simmonds P, Medina JL, Henriquez JA, Mishra N, Wagner J, Tokarz R, Cullen JM, Iadarola MJ, Rice CM, Lipkin WI, Kapoor A.** 2012. Serology-enabled discovery of genetically diverse hepaciviruses in a new host. Journal of virology **86:**6171-6178.
3. **Drexler JF, Corman VM, Muller MA, Lukashev AN, Gmyl A, Coutard B, Adam A, Ritz D, Leijten LM, van Riel D, Kallies R, Klose SM, Gloza-Rausch F, Binger T, Annan A, Adu-Sarkodie Y, Oppong S, Bourgarel M, Rupp D, Hoffmann B, Schlegel M, Kummerer BM, Kruger DH, Schmidt-Chanasit J, Setien AA, Cottontail VM, Hemachudha T, Wacharapluesadee S, Osterrieder K, Bartenschlager R, Matthee S, Beer M, Kuiken T, Reusken C, Leroy EM, Ulrich RG, Drosten C.** 2013. Evidence for novel hepaciviruses in rodents. PLoS pathogens **9:**e1003438.
4. **Quan PL, Firth C, Conte JM, Williams SH, Zambrana-Torrelio CM, Anthony SJ, Ellison JA, Gilbert AT, Kuzmin IV, Niezgoda M, Osinubi MO, Recuenco S, Markotter W, Breiman RF, Kalemba L, Malekani J, Lindblade KA, Rostal MK, Ojeda-Flores R, Suzan G, Davis LB, Blau DM, Ogunkoya AB, Alvarez Castillo DA, Moran D, Ngam S, Akaibe D, Agwanda B, Briese T, Epstein JH, Daszak P, Rupprecht CE, Holmes EC, Lipkin WI.** 2013. Bats are a major natural reservoir for hepaciviruses and pegiviruses. Proceedings of the National Academy of Sciences of the United States of America **110:**8194-8199.
5. **Kapoor A, Simmonds P, Scheel TK, Hjelle B, Cullen JM, Burbelo PD, Chauhan LV, Duraisamy R, Sanchez Leon M, Jain K, Vandegrift KJ, Calisher CH, Rice CM, Lipkin WI.** 2013. Identification of rodent homologs of hepatitis C virus and pegiviruses. mBio **4:**e00216-00213.
6. **Lauck M, Sibley SD, Lara J, Purdy MA, Khudyakov Y, Hyeroba D, Tumukunde A, Weny G, Switzer WM, Chapman CA, Hughes AL, Friedrich TC, O'Connor DH, Goldberg TL.** 2013. A novel hepacivirus with an unusually long and intrinsically disordered NS5A protein in a wild Old World primate. Journal of virology **87:**8971-8981.

7. **Firth C, Bhat M, Firth MA, Williams SH, Frye MJ, Simmonds P, Conte JM, Ng J, Garcia J, Bhuva NP, Lee B, Che X, Quan PL, Lipkin WI.** 2014. Detection of zoonotic pathogens and characterization of novel viruses carried by commensal Rattus norvegicus in New York City. mBio **5:**e01933-01914.
8. **Corman VM, Grundhoff A, Baechlein C, Fischer N, Gmyl A, Wollny R, Dei D, Ritz D, Binger T, Adankwah E, Marfo KS, Annison L, Annan A, Adu-Sarkodie Y, Oppong S, Becher P, Drosten C, Drexler JF.** 2015. Highly divergent hepaciviruses from African cattle. Journal of virology **89:**5876-5882.
9. **Baechlein C, Fischer N, Grundhoff A, Alawi M, Indenbirken D, Postel A, Baron AL, Offinger J, Becker K, Beineke A, Rehage J, Becher P.** 2015. Identification of a Novel Hepacivirus in Domestic Cattle from Germany. Journal of virology **89:**7007-7015.
10. **Scheel TK, Simmonds P, Kapoor A.** 2015. Surveying the global virome: identification and characterization of HCV-related animal hepaciviruses. Antiviral research **115:**83-93.
11. **Pfaender S, Brown RJ, Pietschmann T, Steinmann E.** 2014. Natural reservoirs for homologs of hepatitis C virus. Emerging microbes & infections **3:**e21.
12. **Global Burden of Disease Study C.** 2015. Global, regional, and national incidence, prevalence, and years lived with disability for 301 acute and chronic diseases and injuries in 188 countries, 1990-2013: a systematic analysis for the Global Burden of Disease Study 2013. Lancet **386:**743-800.
13. **Hoofnagle JH.** 1997. Hepatitis C: the clinical spectrum of disease. Hepatology **26:**15S-20S.
14. **Pawlotsky JM.** 2014. New hepatitis C therapies: the toolbox, strategies, and challenges. Gastroenterology **146:**1176-1192.
15. **Bartenschlager R, Frese M, Pietschmann T.** 2004. Novel insights into hepatitis C virus replication and persistence. Advances in virus research **63:**71-180.
16. **Scott C, Griffin S.** 2015. Viroporins: structure, function and potential as antiviral targets. The Journal of general virology **96:**2000-2027.
17. **Carrere-Kremer S, Montpellier-Pala C, Cocquerel L, Wychowski C, Penin F, Dubuisson J.** 2002. Subcellular localization and topology of the p7 polypeptide of hepatitis C virus. Journal of virology **76:**3720-3730.
18. **Isherwood BJ, Patel AH.** 2005. Analysis of the processing and transmembrane topology of the E2p7 protein of hepatitis C virus. The Journal of general virology **86:**667-676.

19. **Chandler DE, Penin F, Schulten K, Chipot C.** 2012. The p7 protein of hepatitis C virus forms structurally plastic, minimalist ion channels. PLoS computational biology **8:**e1002702.
20. **Luik P, Chew C, Aittoniemi J, Chang J, Wentworth P, Jr., Dwek RA, Biggin PC, Venien-Bryan C, Zitzmann N.** 2009. The 3-dimensional structure of a hepatitis C virus p7 ion channel by electron microscopy. Proceedings of the National Academy of Sciences of the United States of America **106:**12712-12716.
21. **Griffin SD, Beales LP, Clarke DS, Worsfold O, Evans SD, Jaeger J, Harris MP, Rowlands DJ.** 2003. The p7 protein of hepatitis C virus forms an ion channel that is blocked by the antiviral drug, Amantadine. FEBS letters **535:**34-38.
22. **Clarke D, Griffin S, Beales L, Gelais CS, Burgess S, Harris M, Rowlands D.** 2006. Evidence for the formation of a heptameric ion channel complex by the hepatitis C virus p7 protein in vitro. The Journal of biological chemistry **281:**37057-37068.
23. **Montserret R, Saint N, Vanbelle C, Salvay AG, Simorre JP, Ebel C, Sapay N, Renisio JG, Bockmann A, Steinmann E, Pietschmann T, Dubuisson J, Chipot C, Penin F.** 2010. NMR structure and ion channel activity of the p7 protein from hepatitis C virus. The Journal of biological chemistry **285:**31446-31461.
24. **Foster TL, Thompson GS, Kalverda AP, Kankanala J, Bentham M, Wetherill LF, Thompson J, Barker AM, Clarke D, Noerenberg M, Pearson AR, Rowlands DJ, Homans SW, Harris M, Foster R, Griffin S.** 2014. Structure-guided design affirms inhibitors of hepatitis C virus p7 as a viable class of antivirals targeting virion release. Hepatology **59:**408-422.
25. **Cook GA, Dawson LA, Tian Y, Opella SJ.** 2013. Three-dimensional structure and interaction studies of hepatitis C virus p7 in 1,2-dihexanoyl-sn-glycero-3-phosphocholine by solution nuclear magnetic resonance. Biochemistry **52:**5295-5303.
26. **OuYang B, Xie S, Berardi MJ, Zhao X, Dev J, Yu W, Sun B, Chou JJ.** 2013. Unusual architecture of the p7 channel from hepatitis C virus. Nature **498:**521-525.
27. **Steinmann E, Penin F, Kallis S, Patel AH, Bartenschlager R, Pietschmann T.** 2007. Hepatitis C virus p7 protein is crucial for assembly and release of infectious virions. PLoS pathogens **3:**e103.

28. **Jones CT, Murray CL, Eastman DK, Tassello J, Rice CM.** 2007. Hepatitis C virus p7 and NS2 proteins are essential for production of infectious virus. Journal of virology **81:**8374-8383.

29. **Madan V, Bartenschlager R.** 2015. Structural and Functional Properties of the Hepatitis C Virus p7 Viroporin. Viruses **7:**4461-4481.

30. **Steinmann E, Pietschmann T.** 2010. Hepatitis C virus p7-a viroporin crucial for virus assembly and an emerging target for antiviral therapy. Viruses **2:**2078-2095.

31. **Pfaender S, Cavalleri JM, Walter S, Doerrbecker J, Campana B, Brown RJ, Burbelo PD, Postel A, Hahn K, Anggakusuma, Riebesehl N, Baumgartner W, Becher P, Heim MH, Pietschmann T, Feige K, Steinmann E.** 2015. Clinical course of infection and viral tissue tropism of hepatitis C virus-like nonprimate hepaciviruses in horses. Hepatology **61:**447-459.

32. **Tanaka T, Kasai H, Yamashita A, Okuyama-Dobashi K, Yasumoto J, Maekawa S, Enomoto N, Okamoto T, Matsuura Y, Morimatsu M, Manabe N, Ochiai K, Yamashita K, Moriishi K.** 2014. Hallmarks of hepatitis C virus in equine hepacivirus. Journal of virology **88:**13352-13366.

33. **Parera M, Martrus G, Franco S, Clotet B, Martinez MA.** 2012. Canine hepacivirus NS3 serine protease can cleave the human adaptor proteins MAVS and TRIF. PloS one **7:**e42481.

34. **Tamura K, Stecher G, Peterson D, Filipski A, Kumar S.** 2013. MEGA6: Molecular Evolutionary Genetics Analysis version 6.0. Molecular biology and evolution **30:**2725-2729.

35. **Thompson JD, Higgins DG, Gibson TJ.** 1994. CLUSTAL W: improving the sensitivity of progressive multiple sequence alignment through sequence weighting, position-specific gap penalties and weight matrix choice. Nucleic acids research **22:**4673-4680.

36. **Biasini M, Bienert S, Waterhouse A, Arnold K, Studer G, Schmidt T, Kiefer F, Cassarino TG, Bertoni M, Bordoli L, Schwede T.** 2014. SWISS-MODEL: modelling protein tertiary and quaternary structure using evolutionary information. Nucleic acids research **42:**W252-258.

37. **Kalita MM, Griffin S, Chou JJ, Fischer WB.** 2015. Genotype-specific differences in structural features of hepatitis C virus (HCV) p7 membrane protein. Biochimica et biophysica acta **1848:**1383-1392.

38. **Humphrey W, Dalke A, Schulten K.** 1996. VMD: visual molecular dynamics. Journal of molecular graphics **14:**33-38, 27-38.

39. **StGelais C, Tuthill TJ, Clarke DS, Rowlands DJ, Harris M, Griffin S.** 2007. Inhibition of hepatitis C virus p7 membrane channels in a liposome-based assay system. Antiviral research **76:**48-58.

40. **Steinmann E, Brohm C, Kallis S, Bartenschlager R, Pietschmann T.** 2008. Efficient trans-encapsidation of hepatitis C virus RNAs into infectious virus-like particles. Journal of virology **82:**7034-7046.

41. **Brohm C, Steinmann E, Friesland M, Lorenz IC, Patel A, Penin F, Bartenschlager R, Pietschmann T.** 2009. Characterization of determinants important for hepatitis C virus p7 function in morphogenesis by using trans-complementation. Journal of virology **83:**11682-11693.

42. **Vieyres G, Brohm C, Friesland M, Gentzsch J, Wolk B, Roingeard P, Steinmann E, Pietschmann T.** 2013. Subcellular localization and function of an epitope-tagged p7 viroporin in hepatitis C virus-producing cells. Journal of virology **87:**1664-1678.

43. **Pietschmann T, Kaul A, Koutsoudakis G, Shavinskaya A, Kallis S, Steinmann E, Abid K, Negro F, Dreux M, Cosset FL, Bartenschlager R.** 2006. Construction and characterization of infectious intragenotypic and intergenotypic hepatitis C virus chimeras. Proceedings of the National Academy of Sciences of the United States of America **103:**7408-7413.

44. **Appel N, Zayas M, Miller S, Krijnse-Locker J, Schaller T, Friebe P, Kallis S, Engel U, Bartenschlager R.** 2008. Essential role of domain III of nonstructural protein 5A for hepatitis C virus infectious particle assembly. PLoS pathogens **4:**e1000035.

45. **Keck ZY, Xia J, Wang Y, Wang W, Krey T, Prentoe J, Carlsen T, Li AY, Patel AH, Lemon SM, Bukh J, Rey FA, Foung SK.** 2012. Human monoclonal antibodies to a novel cluster of conformational epitopes on HCV E2 with resistance to neutralization escape in a genotype 2a isolate. PLoS pathogens **8:**e1002653.

46. **Lindenbach BD, Evans MJ, Syder AJ, Wolk B, Tellinghuisen TL, Liu CC, Maruyama T, Hynes RO, Burton DR, McKeating JA, Rice CM.** 2005. Complete replication of hepatitis C virus in cell culture. Science **309:**623-626.

47. **Dentzer TG, Lorenz IC, Evans MJ, Rice CM.** 2009. Determinants of the hepatitis C virus nonstructural protein 2 protease domain required for production of infectious virus. Journal of virology **83:**12702-12713.

48. **Owsianka A, Tarr AW, Juttla VS, Lavillette D, Bartosch B, Cosset FL, Ball JK, Patel AH.** 2005. Monoclonal antibody AP33 defines a broadly neutralizing epitope on the hepatitis C virus E2 envelope glycoprotein. Journal of virology **79:**11095-11104.

49. **Altschul SF, Madden TL, Schaffer AA, Zhang J, Zhang Z, Miller W, Lipman DJ.** 1997. Gapped BLAST and PSI-BLAST: a new generation of protein database search programs. Nucleic acids research **25:**3389-3402.

50. **Pearson WR.** 1991. Searching protein sequence libraries: comparison of the sensitivity and selectivity of the Smith-Waterman and FASTA algorithms. Genomics **11:**635-650.

51. **Smith DB, Bukh J, Kuiken C, Muerhoff AS, Rice CM, Stapleton JT, Simmonds P.** 2014. Expanded classification of hepatitis C virus into 7 genotypes and 67 subtypes: updated criteria and genotype assignment web resource. Hepatology **59:**318-327.

52. **Simmonds P, Bukh J, Combet C, Deleage G, Enomoto N, Feinstone S, Halfon P, Inchauspe G, Kuiken C, Maertens G, Mizokami M, Murphy DG, Okamoto H, Pawlotsky JM, Penin F, Sablon E, Shin IT, Stuyver LJ, Thiel HJ, Viazov S, Weiner AJ, Widell A.** 2005. Consensus proposals for a unified system of nomenclature of hepatitis C virus genotypes. Hepatology **42:**962-973.

53. **Nieva JL, Madan V, Carrasco L.** 2012. Viroporins: structure and biological functions. Nature reviews. Microbiology **10:**563-574.

54. **Pavlovic D, Neville DC, Argaud O, Blumberg B, Dwek RA, Fischer WB, Zitzmann N.** 2003. The hepatitis C virus p7 protein forms an ion channel that is inhibited by long-alkyl-chain iminosugar derivatives. Proceedings of the National Academy of Sciences of the United States of America **100:**6104-6108.

55. **Griffin S.** 2014. "Too little, too late?" Will inhibitors of the hepatitis C virus p7 ion channel ever be used in the clinic? Future medicinal chemistry **6:**1893-1907.

56. **Carrere-Kremer S, Montpellier C, Lorenzo L, Brulin B, Cocquerel L, Belouzard S, Penin F, Dubuisson J.** 2004. Regulation of hepatitis C virus polyprotein processing by signal peptidase involves structural determinants at the p7 sequence junctions. The Journal of biological chemistry **279:**41384-41392.

57. **Scull MA, Schneider WM, Flatley BR, Hayden R, Fung C, Jones CT, van de Belt M, Penin F, Rice CM.** 2015. The N-terminal Helical Region of the Hepatitis C Virus p7 Ion Channel Protein Is Critical for Infectious Virus Production. PLoS pathogens **11:**e1005297.

58. **StGelais C, Foster TL, Verow M, Atkins E, Fishwick CW, Rowlands D, Harris M, Griffin S.** 2009. Determinants of hepatitis C virus p7 ion channel function and drug sensitivity identified in vitro. Journal of virology **83:**7970-7981.

59. **Sakai A, Claire MS, Faulk K, Govindarajan S, Emerson SU, Purcell RH, Bukh J.** 2003. The p7 polypeptide of hepatitis C virus is critical for infectivity and contains functionally important genotype-specific sequences. Proceedings of the National Academy of Sciences of the United States of America **100:**11646-11651.

60. **Steinmann E, Whitfield T, Kallis S, Dwek RA, Zitzmann N, Pietschmann T, Bartenschlager R.** 2007. Antiviral effects of amantadine and iminosugar derivatives against hepatitis C virus. Hepatology **46:**330-338.

61. **Crooks GE, Hon G, Chandonia JM, Brenner SE.** 2004. WebLogo: a sequence logo generator. Genome research **14:**1188-1190.

62. **von Heijne G.** 1990. The signal peptide. The Journal of membrane biology **115:**195-201.

63. **von Heijne G.** 1998. Life and death of a signal peptide. Nature **396:**111, 113.

A)


```
NPHV p7 Consensus YLSDTMRLIALSYIADDSLLYALLFYCVIYFTPSRVPPFCVFVYYWKFSLAFMVLALPHRAWA
                 *** ********* ****** ** *** ** * ** ****** ***** *** **********
```

B)

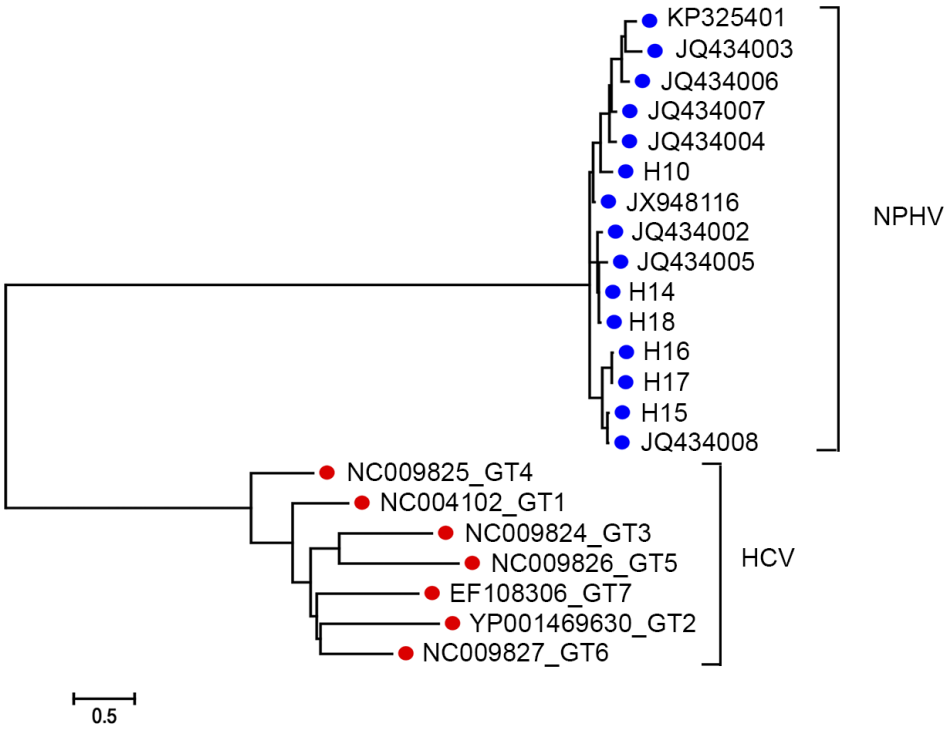

A) Sequence similarity

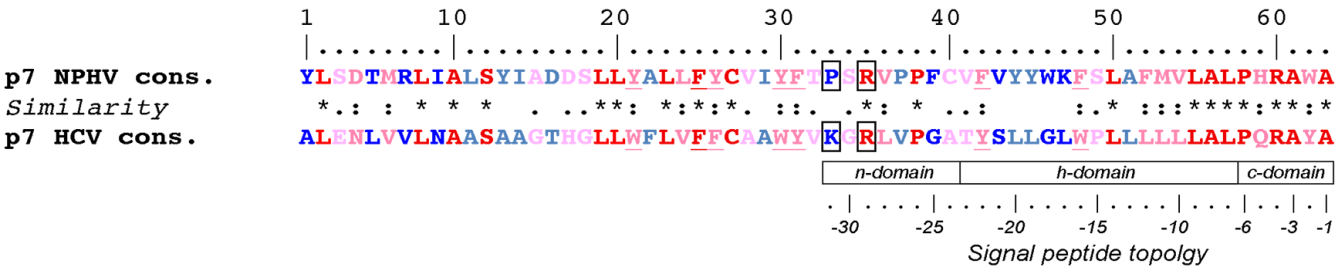

B) Homology monomer models of p7 NPHV

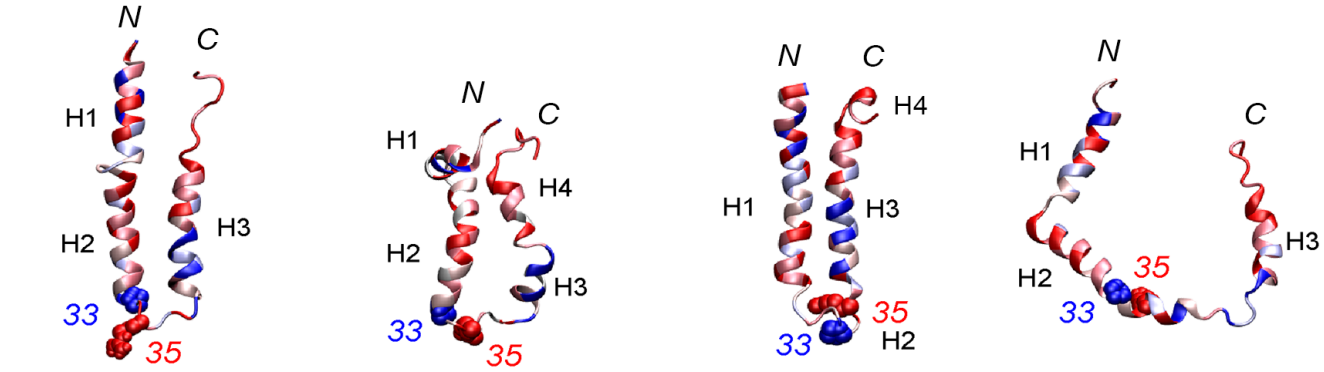

Montserret et al. (2010) *Cook et al. (2013)* *Foster et al. (2014)* *Ouyang et al. (2013)*

C) Homology hexamer models of p7 NPHV

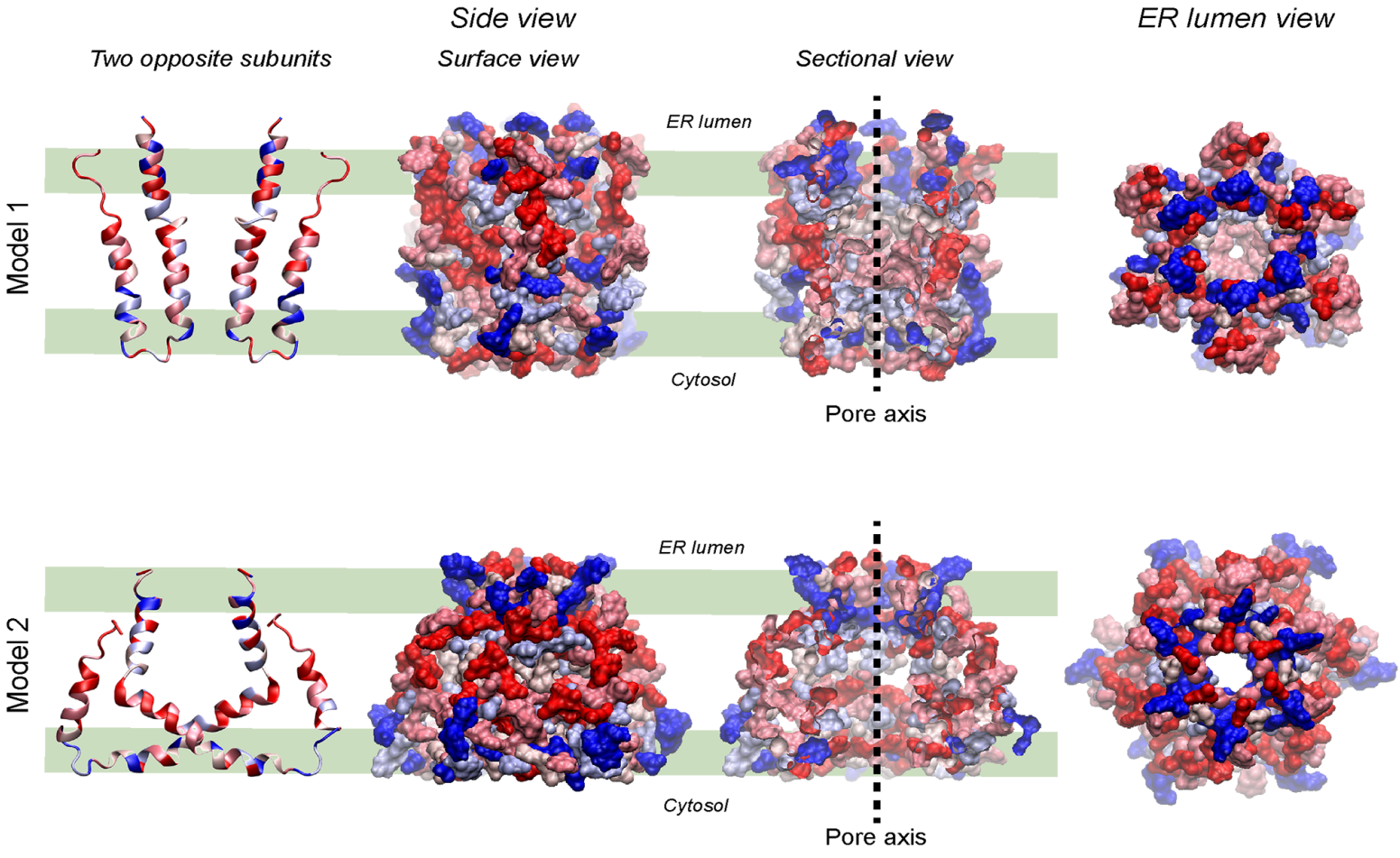

A)

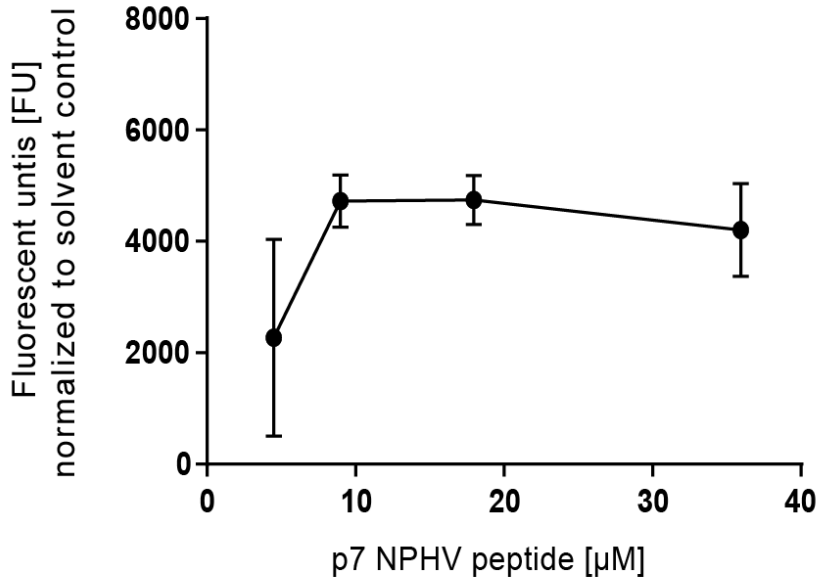
Fluorescent untis [FU]
normalized to solvent control
8000
6000
4000
2000
0
0
10
20
30
40
p7 NPHV peptide [µM]

B)

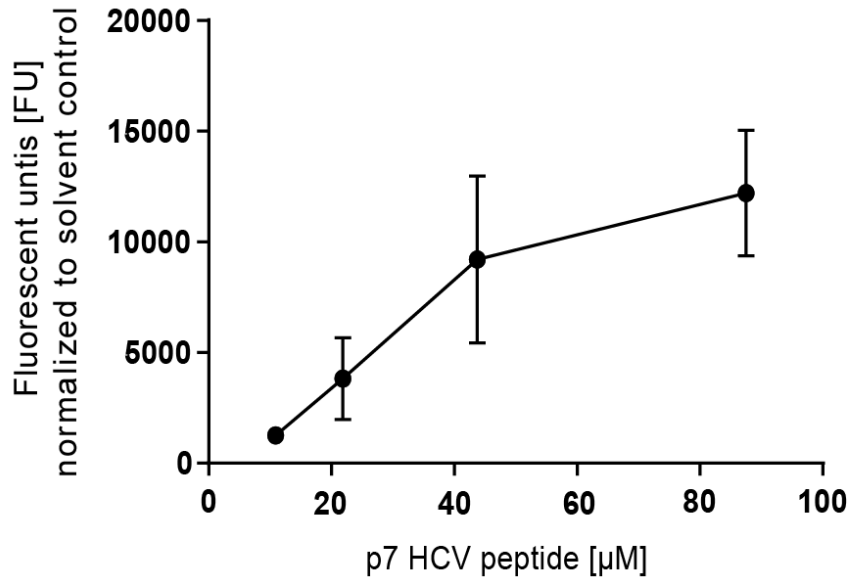
Fluorescent untis [FU]
normalized to solvent control
20000
15000
10000
5000
0
0
20
40
60
80
100
p7 HCV peptide [µM]

C)

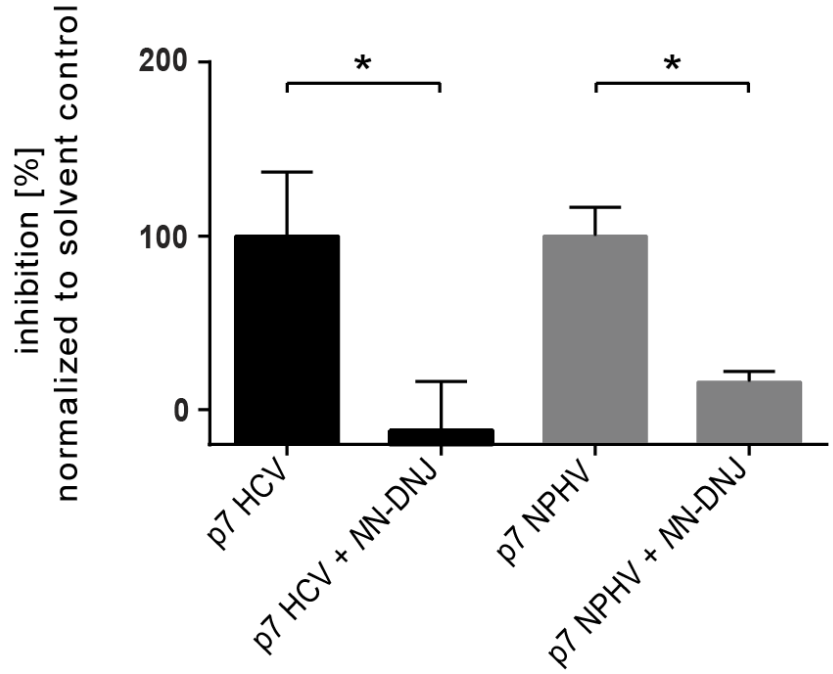
inhibition [%]
normalized to solvent control
200
100
0
*
*
p7 HCV
p7 HCV + NN-DNJ
p7 NPHV
p7 NPHV + NN-DNJ

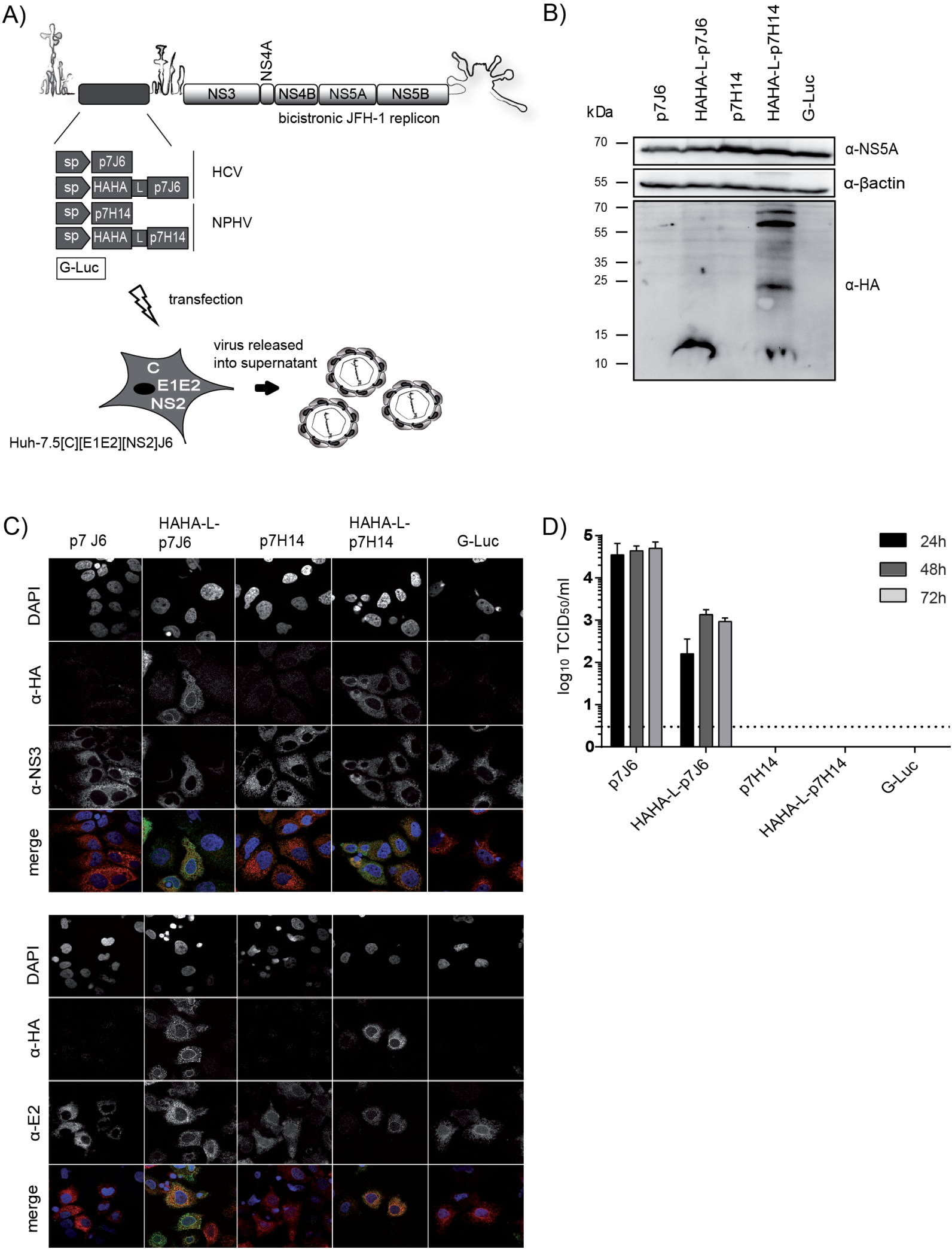
A)
NS4A
NS3
NS4B
NS5A
NS5B
bicistronic JFH-1 replicon
sp
p7J6
HAHA
L
HCV
p7H14
NPHV
G-Luc
transfection
virus released
into supernatant
C
E1E2
NS2
Huh-7.5[C][E1E2][NS2]J6
B)
kDa
p7J6
HAHA-L-p7J6
p7H14
HAHA-L-p7H14
G-Luc
70
55
35
25
15
10
α-NS5A
α-βactin
α-HA
C)
p7 J6
HAHA-L-p7J6
p7H14
HAHA-L-p7H14
G-Luc
DAPI
α-HA
α-NS3
merge
α-E2
D)
log10 TCID50/ml
24h
48h
72h
p7J6
HAHA-L-p7J6
p7H14
HAHA-L-p7H14
G-Luc

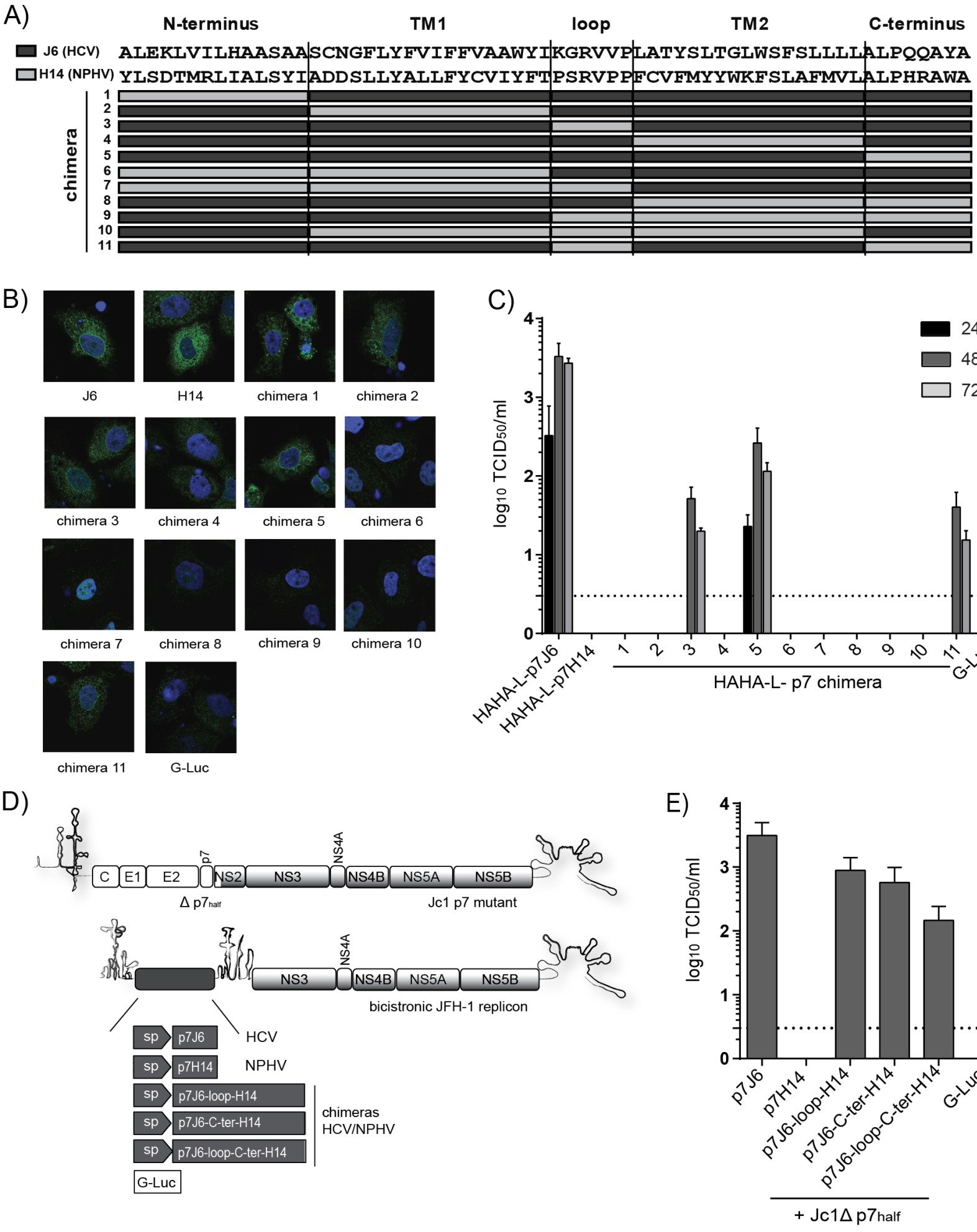
A)
N-terminus
TM1
loop
TM2
C-terminus
J6 (HCV)
H14 (NPHV)
ALEKLVILHAASAASCNGFLYFVIFFVAAWYIKGRVVPLATYSLTGLWSFSLLLLALPQQAYA
YLSDTMRLIALSYIADDSLLYALLFYCVIYFTPSRVPPFCVFMYYWKFSLAFMVLALPHRAWA
chimera
1
2
3
4
5
6
7
8
9
10
11
B)
J6
H14
chimera 1
chimera 2
chimera 3
chimera 4
chimera 5
chimera 6
chimera 7
chimera 8
chimera 9
chimera 10
chimera 11
G-Luc
C)
24h
48h
72h
log10 TCID50/ml
0
1
2
3
4
HAHA-L-p7J6
HAHA-L-p7H14
1
2
3
4
5
6
7
8
9
10
11
G-Luc
HAHA-L- p7 chimera
D)
C
E1
E2
p7
NS2
NS3
NS4A
NS4B
NS5A
NS5B
Δ p7half
Jc1 p7 mutant
bicistronic JFH-1 replicon
sp
p7J6
HCV
p7H14
NPHV
p7J6-loop-H14
p7J6-C-ter-H14
p7J6-loop-C-ter-H14
chimeras
HCV/NPHV
G-Luc
E)
log10 TCID50/ml
0
1
2
3
4
p7J6
p7H14
p7J6-loop-H14
p7J6-C-ter-H14
p7J6-loop-C-ter-H14
G-Luc
+ Jc1Δ p7half

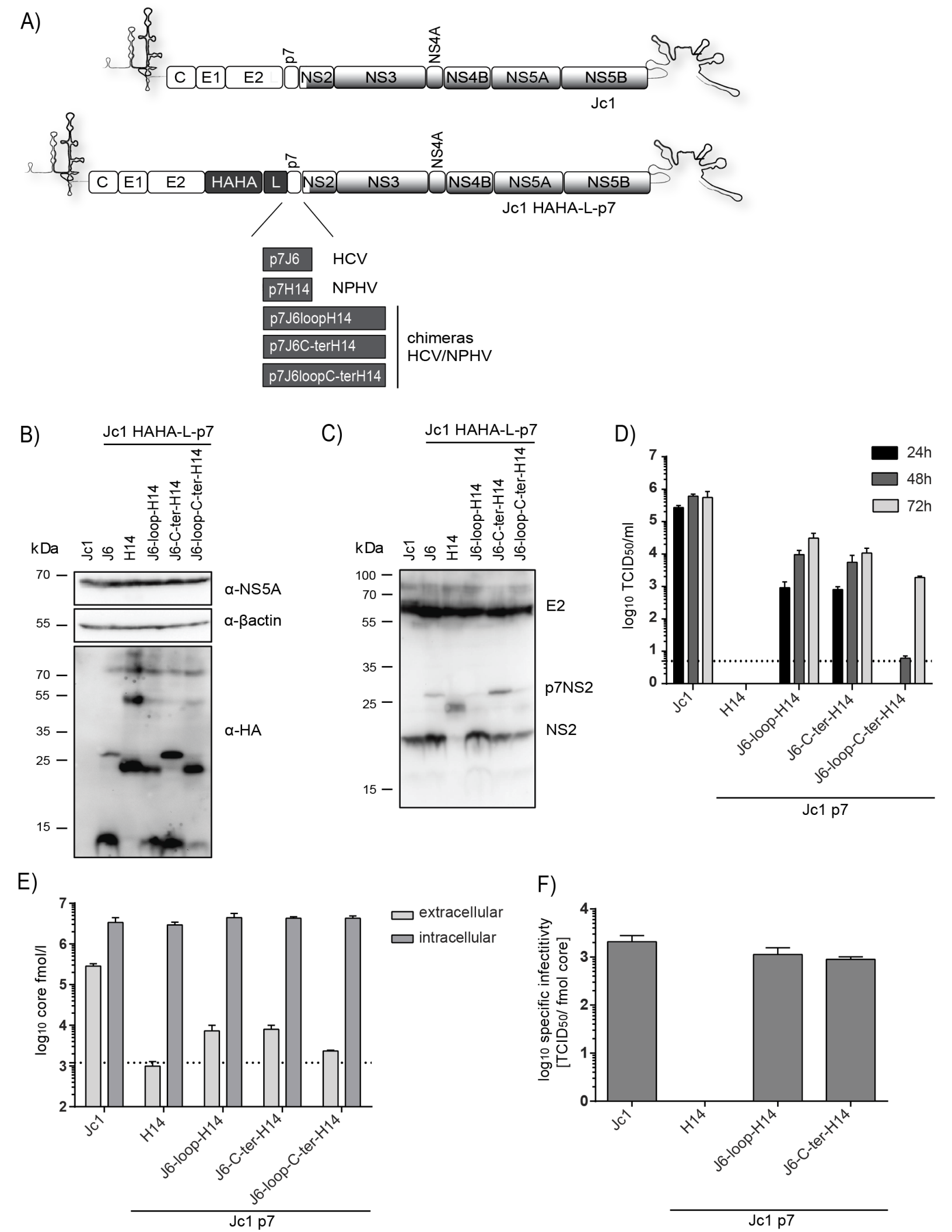
A)
C
E1
E2
p7
NS2
NS3
NS4A
NS4B
NS5A
NS5B
Jc1
HAHA
L
Jc1 HAHA-L-p7
p7J6
HCV
p7H14
NPHV
p7J6loopH14
p7J6C-terH14
p7J6loopC-terH14
chimeras
HCV/NPHV
B)
Jc1 HAHA-L-p7
kDa
Jc1
J6
H14
J6-loop-H14
J6-C-ter-H14
J6-loop-C-ter-H14
70
55
35
25
15
α-NS5A
α-βactin
α-HA
C)
Jc1 HAHA-L-p7
kDa
100
70
55
35
25
15
E2
p7NS2
NS2
D)
24h
48h
72h
log10 TCID50/ml
Jc1 p7
E)
extracellular
intracellular
log10 core fmol/l
Jc1 p7
F)
log10 specific infectitivty
[TCID50/ fmol core]
Jc1 p7

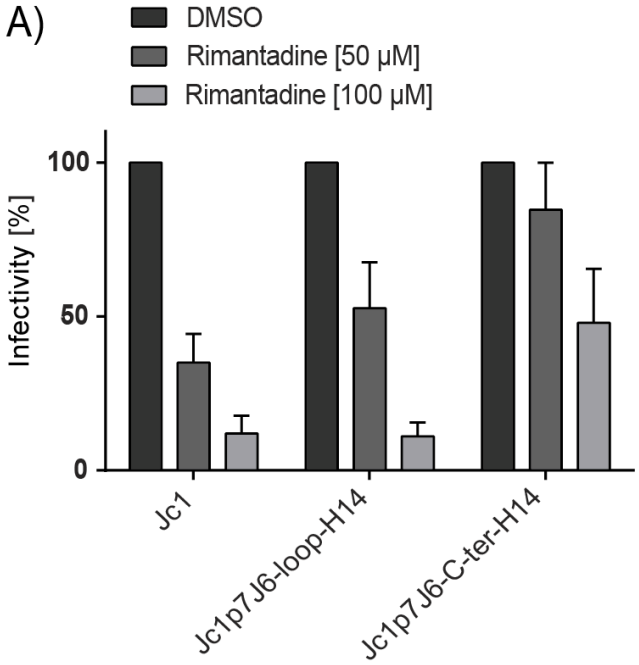
A)
DMSO
Rimantadine [50 µM]
Rimantadine [100 µM]
Infectivity [%]
100
50
0
Jc1
Jc1p7J6-loop-H14
Jc1p7J6-C-ter-H14

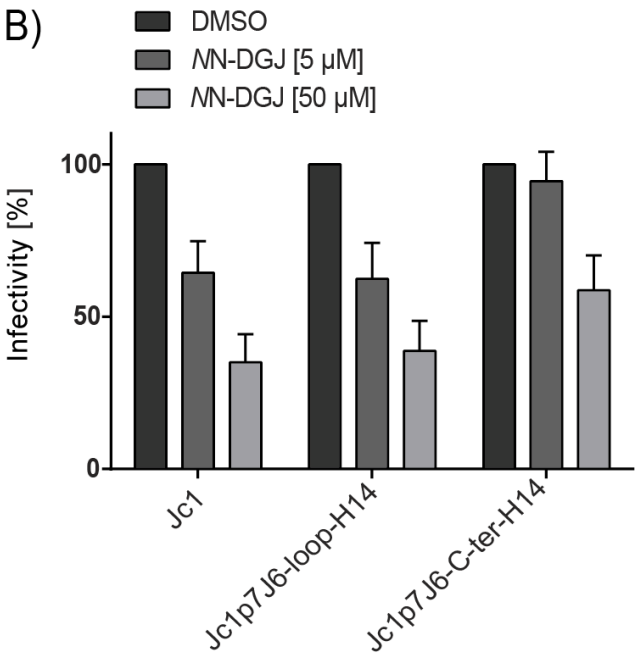
B)
DMSO
NN-DGJ [5 µM]
NN-DGJ [50 µM]
Infectivity [%]
100
50
0
Jc1
Jc1p7J6-loop-H14
Jc1p7J6-C-ter-H14

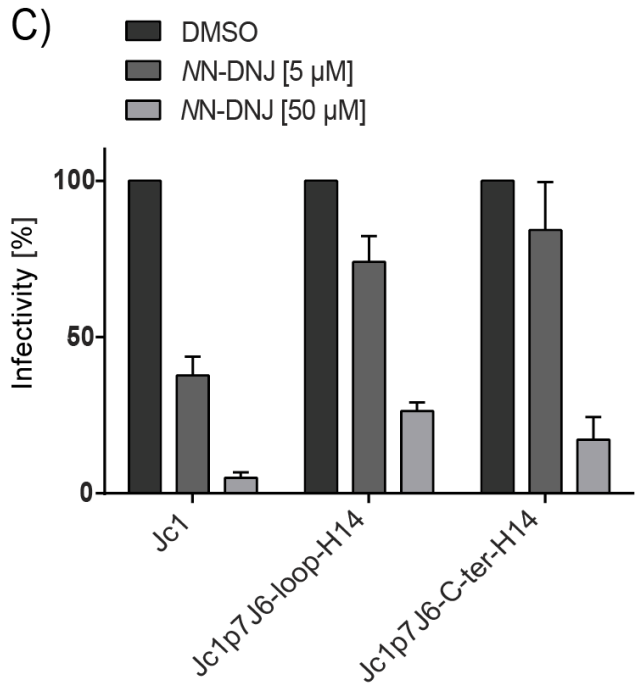
C)
DMSO
NN-DNJ [5 µM]
NN-DNJ [50 µM]
Infectivity [%]
100
50
0
Jc1
Jc1p7J6-loop-H14
Jc1p7J6-C-ter-H14